ABSTRACT

Title of Document: EVALUATION OF THE NASA MICROWAVE RADIATIVE TRANSFER MODEL FOR SOIL MOISTURE ESTIMATION USING AQUARIUS BRIGHTNESS TEMPERATURE OBSERVATIONS OVER THE CONTINENTAL UNITED STATES

Saad Bin Tarik, Masters of Science, 2014

Directed By: Dr. Barton A. Forman, Department of Civil and Environmental Engineering

The implications of near-surface soil moisture (~5 cm) variability in land surface processes and land-atmosphere interactions is important in regional and global scale climatology since it controls the partitioning of precipitation and radiation fluxes that play a crucial role in dictating weather and climate. Passive microwave (PMW) remote sensing is an increasingly popular approach to measure soil moisture because of its global coverage of the Earth. This study evaluates the performance of the NASA Goddard Earth Observing System, Version 5 (GEOS-5) radiative transfer model (RTM) using Aquarius brightness temperature (Tb) observations with the eventual goal of integrating the RTM into a data assimilation (DA) framework for the purpose of improved soil moisture estimation. Statistics were calculated from two plus years of observations across different climate regions of the United States. Seasonal variations of soil moisture were also investigated. Results suggest the RTM reasonably reproduces Aquarius Tbs, but that systematic biases exist, which must be mitigated prior to inclusion into the DA framework.

EVALUATION OF THE NASA MICROWAVE RADIATIVE TRANSFER MODEL FOR SOIL MOISTURE ESTIMATION USING AQUARIUS BRIGHTNESS TEMPERATURE OBSERVATIONS OVER THE CONTINENTAL UNITED STATES.

By

Saad Bin Tarik

Thesis submitted to the Faculty of the Graduate School of the
University of Maryland, College Park, in partial fulfillment
of the requirements for the degree of
Masters of Science
2014

Advisory Committee:
Dr. Barton A. Forman, Chair
Dr. Richard H. McCuen
Dr. Kaye L. Brubaker

Dedication

To

My Parents

Acknowledgement

It is my immense pleasure to express my gratitude to those whose support and cooperation helped me to complete this study. I would like to thank my advisor and mentor Professor Barton A. Forman for his incredible support, encouragement and advice from the very beginning of my graduate study. I do appreciate his supervision and guidance that he provided during the study period and especially his tutelage on advanced computational techniques in order to properly conduct a research.

I would also like to thank Dr. Gabriëlle J. M. DeLannoy and Dr. Rolf H. Reichle, hydrologists at NASA Goddard Space Flight Center, Greenbelt, MD, for processing the radiative transfer model to estimate brightness temperature and for making them available for this study.

I would like to thank Professor Richard H. McCuen and Professor Kaye L. Brubaker for their service as thesis committee members and also for reviewing this document. I am also grateful to them for teaching me advanced statistical methods and GIS analysis for hydrologic modeling through the courses they offered, which was a tremendous learning experience. These courses helped me understand real-world significances and applications of statistics and GIS techniques in hydrology, which was helpful during this study.

Special thanks goes to my beloved family members whose unwavering and persistent support and encouragement helped me to continue my graduate study.

Last but not the least, I would like to thank my fellow classmate and research colleague Yuan Xue for reviewing this document as well as for her valuable comments to improve this thesis.

Table of Contents

List of Figures

List of Tables

List of Acronyms and Abbreviations

CLSM	Catchment Land Surface Model
DA	Data Assimilation
EASE	Equal Area Scalable Earth Grid
ENSO	El-Niño Southern Oscillation
ESA	European Space Agency
GEOS-5	Goddard Earth Observing System, Version 5
GLACE	Global Land-Atmosphere Coupling Experiment
HDF5	Hierarchical Data Format
JPL	Jet Propulsion Laboratory
MERRA	Modern-Era Retrospective analysis for Research and Analysis
NASA	National Aeronautics and Space Administration
NOAA	National Oceanic and Atmospheric Administration
PMW	Passive Microwave
RADAR	Radio Detection and Ranging
RMSE	Root Mean Squared Error
RTM	Radiative Transfer Model
SAC-D	Satéllite de Aplicaciones Científicas
SMOS	Soil Moisture Ocean Salinity
SMAP	Soil Moisture Active Passive
SSS	Sea Surface Salinity
Tb	Brightness Temperature
TDR	Time Domain Reflectometry

US	United States
USCRN	United States Climate Reference Network
WBAN	Weather Bureau Army Navy
VWC	Volumetric Water Content

Chapter 1: Introduction and Motivation

1.1 Motivation and Background

Soil moisture plays a key role in hydrologic, meteorologic, and land surface processes (Cashion et al., 2005; Qiu et al., 2013; Su et al., 2013). Generally, soil moisture is defined as the water that is stored in the root zone (approximately top meter of soil), which interacts with the overlying atmosphere through evapotranspiration and precipitation (Pan et al., 2003). It strongly affects the surface energy and precipitation fluxes by acting as a first-order control on their partitioning (Brubaker and Entekhabi, 1995; Corradini, 2014; Delworth and Manabe, 1989; Entekhabi et al., 1996; Moradkhani, 2008; Reichle et al., 2002; Xia et al., 2014). Soil moisture-precipitation feedback plays a crucial role in controlling weather patterns and land surface processes, which are particularly evident in transitional climate regions (Koster et al., 2004, 2003; Seneviratne et al., 2010). Studies on soil moisture and related land-atmosphere interactions show it also affects other factors in the atmosphere such as humidity, temperature, and wind flow (Zaitchik et al., 2013).

Frequent monitoring of soil moisture allows meteorologists, hydrologists, and climatologists to characterize and forecast hydrologic and climatic events such as precipitation, floods, droughts, and streamflow (Brocca et al., 2013a, 2013b; Cashion et al., 2005; Koster et al., 2010). However, soil moisture is highly variable in space and time (Ahmad et al., 2010), which impacts the uncertainty in its prediction. Further, this variability (and uncertainty) drives much of the large-scale anomalies in precipitation (Reichle et al., 2002) and has significant impacts on atmospheric behavior at seasonal and

annual timescales (Cashion et al., 2005) as well as long-term prediction of climatic conditions (Walker and Houser, 2001). Therefore it is of great importance to monitor and characterize soil moisture variability over space and time with precision across high-frequency (~daily) timescales (Houser et al., 1998).

Ground-based sensors are often installed to monitor soil moisture at a local scale (on the order of centimeters) that provide higher temporal (sub-hourly) frequency soil moisture measurements, but do not provide measurements over a large spatial domain. Since soil moisture and large-scale land atmosphere interactions operate over larger (on the order of kilometers) scales, ground-based measurement of point scale soil moisture is not always sufficient to model its spatial variability. Moreover, installing and maintaining ground-based sensors to be operational everywhere at all times would be both expensive and challenging.

To overcome this issue, remote sensing measurements, which are generally collected by sensors on-board an aircraft or a satellite, possess significant advantages over traditional in-situ (i.e., point-scale) measurements of many hydrologic state variables (Schultz and Engman, 2000) such as soil moisture variability over a large area and long time periods. These sensors are typically active or passive microwave sensors that use the principle of the interaction between water particles and the photons emitted from the energy source at microwave frequencies (Dorigo et al., 2010). However, direct measurement of soil moisture (and its variability) is not possible using microwave sensors. Rather, they are inferred from brightness temperature (Tb) observations that vary with the near-surface surface soil moisture content (Jackson, 1993, 2001). Tb itself is a function of surface soil temperature, which is also highly variable like near-surface soil

moisture (Schmugge et al., 2002; Wang and Choudhury, 1981). However, retrieval of microwave emission is only limited to top 5 cm of the soil surface for L-band (1.4 GHz) radiometers (Kerr et al., 2001; Leroux et al., 2013).

The Aquarius (Le Vine et al., 2007) satellite mission was launched in June, 2011, in order to monitor sea surface salinity (SSS) from space. The science objectives of Aquarius include better understanding of the movement of the Earth's freshwater resources as well as interactions between the water cycle and ocean circulation, which require seasonal monitoring of the sea surface salinity over many years. The Aquarius instrument consists of a combined active/passive L-band microwave radiometer from which brightness temperature is inferred from the microwave emissions from the Earth's surface. Utilizing the instrument's microwave radiometer, this study focuses on brightness temperature observed due to soil moisture variability over the Earth's land surface rather than SSS as originally envisioned by Aquarius' creators.

A zero-order (tau-omega) radiative transfer model (RTM) (De Lannoy et al., 2013) is evaluated in this study using Aquarius Tb observations from numerous locations across the contiguous United States. These study locations are selected based on colocation between United States Climate Reference Network (USCRN) (Heim, 2001; Vose and Menne, 2004; Vose et al., 2005) stations and Aquarius satellite instrument observations. The RTM is fed by parameters from the Goddard Earth Observing System, version 5 (GEOS-5) Catchment Land Surface Model (CLSM) (Koster et al., 2000). The output from the RTM consists of L-band Tb predictions. The study conducted here evaluates the performance of a NASA RTM to reproduce Aquarius Tbs with the eventual (future) goal of improving model estimates of soil moisture.

Another focus of this study is to investigate how soil moisture variability is impacted by regional climate type. The contiguous United States consists of several different climate classes based on Köppen Climate Classification (Kottek et al., 2006; Peel, 2007) ranging from humid to dry continental climates. In order to investigate soil moisture variability as a function of climate class, the performance of the RTM is evaluated across a variety of Köppen Climate Classes across the United States.

The overarching goal of this study is to eventually integrate remotely sensed Tb and predicted Tb (via a radiative transfer model) into a data assimilation (DA) framework. Data assimilation is a useful technique that provides improved knowledge of state variables than either the observations or models alone through the reduction of state variable uncertainty (Forman et al., 2012; Moradkhani, 2008; Sahoo et al., 2013). A DA framework improves state estimates by merging available information from both models and measurements (Forman et al., 2012; McLaughlin, 2002) and has been successfully applied to soil moisture studies (Crow and Wood, 2005; Margulis et al., 2002). Information and experience gleaned from this current study will eventually be used in the proposed DA framework for future study.

1.2 Objectives and Scopes of the Study

Motivated by the realization that soil moisture variability should be monitored and modeled frequently to better understand and predict its dynamics, this study will explore the following research questions:

1. How do L-band Tb measurements and RTM predictions vary seasonally/annually at selected study areas?

2. How can L-band Tb variability be characterized by Köppen climate classifications across continental US?
3. How do the GEOS-5 RTM Tb predictions perform compared to Aquarius Tb observations?
4. How do Aquarius Tb observations compare to the USCRN near surface (top 5 cm) volumetric soil moisture content time series?

These research questions are explored in order to find potential solutions that better reflect the soil moisture variability across the study area.

In order to investigate these research questions the Tb observations from Aquarius will be evaluated using a time series comparison with volumetric water content (VWC) from the existing USCRN station locations. This will improve the understanding of Tb retrieval performance from the passive microwave radiometers on board Aquarius. In addition, the evaluation of Tb prediction from the GEOS-5 RTM will be helpful in future DA studies of Tb assimilation from Aquarius in order to better estimate soil moisture conditions.

1.3 Organization of the Thesis

This thesis is organized into five chapters and an overview of each chapter is provided below:

- Chapter 1: This chapter provides the motivation and background information for this study. It provides basic information about soil moisture and its measurement, necessity and advantages of using remote sensing relative to in-situ measurements, an overview of the Aquarius satellite, the radiative transfer

model, and USCRN data. It also includes the objectives and scopes of the study.

- Chapter 2: Provides a literature review on soil moisture, its measurements, and soil moisture induced land-atmospheric interactions. It includes basics of remote sensing, a brief discussion of the different types of sensors, details about soil moisture remote sensing, and an overview of the Aquarius satellite. Details of the radiative transfer model, Tb predictions and in-situ measurement of volumetric water content by USCRN are also included here. Discussions about Köppen climate classes across the US are also provided.
- Chapter 3: Details of the study area and the distribution of climate classes across the domain are given. Further, discussions on Aquarius observations and RTM predictions are provided here. A detailed methodology is discussed along with statistics computed as part of the evaluation are also included in this chapter.
- Chapter 4: This chapter includes the results from statistical analyses and related discussions.
- Chapter 5: This final chapter includes concluding remarks as well as limitations of the study. Recommendations for future research are also provided.

Chapter 2: Literature Review

2.1 Soil Moisture

2.1.1 Definition

Soil moisture is the water held between the particles of soil in the unsaturated zone (i.e., vadose zone) (Hillel, 1998). The unsaturated zone extends from the land surface down to the ground water table (or saturated zone). Soil water is bound to the soil particles by the molecular forces of adhesion and cohesion (Tindall and Kunkel, 1999). Water enters the soil through precipitation and agricultural applications (e.g., irrigation) and re-enters the atmosphere through evaporation from soil and transpiration from plants. In practice, only a fraction of the soil moisture can be measured and considered with reference to a given soil volume (Seneviratne et al., 2010). The distribution of soil moisture is not homogenous but rather highly variable in space and time (Famiglietti et al., 1999).

2.1.2 Measurement of Soil Moisture

There are several methods for measuring soil moisture content. These methods include in situ soil moisture sensors as well as measurements from space using remote sensors. Brief descriptions of such methods are given below.

2.1.2.1 Ground-based Measurements

There are destructive and non-destructive methods for in-situ soil moisture measurements. Destructive methods use a soil sample taken from the field and directly measure the water content while non-destructive methods use sensors that are permanently placed in the soil (Kutilek and Nielsen, 1994). Destructive methods disturb

the existing soil profile each time a sample is collected. Repetitive sample collection destroys the sample area making long-term sampling infeasible. On the other hand, non-destructive methods allow long-term repetitive sampling without altering the soil profile.

Measurements of in situ soil moisture content are further classified into direct and indirect measurements. The mass of the soil water can be obtained from direct measurements while indirect measurements measure some physical property of the soil that is dependent on soil water content (Kutilek and Nielsen, 1994). Specific types of soil moisture measurements are discussed in further detail below.

Gravimetric Measurement: This is a direct and destructive procedure for the measurement of soil water content. This method is often used as a standard for constructing calibration curves for indirect measurements (Kutilek and Nielsen, 1994) despite the drawbacks of destructive measurements. Soil samples are extracted from the field and weighed, then dried in an oven and weighed again. The difference in mass is used to compute the soil moisture content.

Capacitance Methods: This is an indirect approach that uses the dielectric permittivity of soil to derive soil moisture content (Seneviratne et al., 2010). The dielectric constant of water is about 80 [-] and that of dry soil is about 3.5 [-] (Jackson and Schmugge, 1989; Schmugge and Jackson, 1993). Time domain reflectometry (TDR) and soil capacitance sensors use this method, which are based on electromagnetic techniques. However, TDR sensors typically provide higher accuracy than the capacitance sensors (Robinson et al., 2008).

Neutron Probes: This process uses a radiation source of fast neutrons that are attenuated when they interact with the medium surrounding the source (Kutilek and

Nielsen, 1994). Neutrons collide with the nuclei of the atoms in the surrounding soil and are eventually attenuated by the hydrogen nuclei present in the soil water. The neutrons reach thermal velocities (i.e., low-energy neutrons), which are detected by the detectors from which volumetric water content can be obtained via a calibration curve (Jury et al., 1991).

Other indirect sensors used to measure soil moisture content include electric resistance measurements, heat pulse sensors, fiber optic sensors, and gamma ray scanners (Hillel, 1998; Robinson et al., 2008; Robock et al., 2000).

2.1.2.2 Remote Sensing Measurement

Remote sensing is the process of acquiring data or information from an object without direct contact. It utilizes upwelling electromagnetic radiation (both reflected and emitted) from the land surface in order to estimate land surface parameters (Schmugge et al., 2002; Schultz and Engman, 2000). A remote sensing instrument is a sensor that detects electromagnetic radiation from the land surface. Active and passive microwave sensors are the most common types of instruments that are used in remote sensing of soil mositure; these sensors are typically placed on board an airplane or Earth-orbitting satellite in order to measure the upwelling radiation. Remote sensing, especially satellite-based remote sensing, provides a greater advantage over in situ soil measurement because of its large spatial coverage (Jackson, 1993). Remote sensing of soil moisture using different sensors is described in subsequent sections.

Active sensors (such as RADAR) send their own electromagnetic energy that interacts with the terrain and the backscattered energy is then recorded by the receiver. Passive sensors, unlike active sensors, are dependent on the Sun's electromagnetic energy

that is reflected or emitted from the Earth's surface (Jensen, 2007). The large difference between the dielectric constant of water and dry soil (80 for water and 3.5 for dry soil (Schmugge and Jackson, 1993; Schmugge et al., 2002)) results in a large emissivity contrast (0.6 for water and 0.95 for dry soil (Njoku and Entekhabi, 1996; Schmugge and Jackson, 1993; Schmugge et al., 2002)) at microwave frequencies. This is the principle that is utilized in remote sensing of soil moisture (Schmugge et al., 2002). Once the backscattered energy is measured by the radiometers, the large contrast in emissivity is inferred by brightness temperature (Tb) which is defined as (Chaouch et al., 2013; Njoku and Entekhabi, 1996; Schmugge et al., 2002):

$$T_b = \epsilon * T_s \qquad 2\text{-}1$$

where $\epsilon = [0 \quad 1]$ is the emissivity of the soil and T_s [K] is the surface temperature of the soil (a.k.a. physical temperature). Further, the presence of water in the soil results in more evaporative cooling, hence the surface temperature is reduced and a lower brightness temperature is observed. In contrast, the absence of water results in higher brightness temperatures due to the lack of evaporative cooling.

Soil brightness temperature is also affected by some features of the land surface such as soil roughness (Choudhury et al., 1979; Tsang and Newton, 1982), microwave attenuation by overlying vegetation canopy, emission of microwave radiation by overlying vegetation (De Lannoy et al., 2013; Jackson and Schmugge, 1991, 1989; Jackson et al., 1982; Pampaloni and Paloscia, 1986; Schmugge and Jackson, 1993; Schmugge et al., 2002), and surface heterogeneity (Tsang et al., 1975). It has been found that longer wavelengths can penetrate deeper into (or be emitted from deeper) soil

(Cashion et al., 2005) and are also less affected (i.e., more transparent) by vegetation and cloud cover.

Schmugge et al. (2002) listed four unique advantages of using microwave frequencies in remote sensing of soil moisture, which include (1) all weather capability of capturing backscattered energy from the surface, (2) semi-transparency of vegetation cover that enables observation from the underlying surface soil, (3) microwave measurements are sensitive to the presence of water, and (4) measurements of related dielectric properties can be made both at day and night. Low frequency radiometers (Jensen, 2007) (e.g., L-band, $\lambda = 23$ cm, $\nu = 1.4$ GHz) are most frequently used in satellite remote sensing of soil moisture.

2.1.3 Land-Atmosphere Interactions

Soil moisture is a dominant land surface variable that plays a crucial role in land-atmosphere interactions by partitioning the precipitation, runoff, and net radiation (Dirmeyer et al., 2013; Famiglietti et al., 1999; Seneviratne et al., 2010). It is a major source of water in the atmosphere through evaporation from land, open water, and transpiration from plants. Evapotranspiration returns nearly 60 percent of the precipitation that falls on land back to the atmosphere (Oki and Kanae, 2006). Hence soil moisture variability has a profound influence on climate variability (Koster et al., 2011; Santanello et al., 2013) and prediction (Guo et al., 2012; Koster et al., 2006).

The land water balance for a surface soil layer can be expressed as:

$$\frac{dS}{dt} = P - E - R_s - R_g \qquad 2\text{-}2$$

where $\frac{dS}{dt}$ is the change in water storage in the soil layer, P is the precipitation input, E is the evapotranspiration from the soil and plants, R_s is the surface runoff, and R_g is the drainage component that later contributes to the base flow. Analogously, the land energy balance can be expressed (Shuttleworth, 2012) as

$$\frac{dH}{dt} = R_n - \lambda E - S - G \qquad 2\text{-}3$$

where $\frac{dH}{dt}$ is the change in energy in the given soil layer, R_n is the net radiation flux, λE is the latent heat flux, S is the sensible heat flux, and G is the ground heat flux. The net radiation is then defined as:

$$R_n = SW_{in} - SW_{out} + LW_{in} - LW_{out} \qquad 2\text{-}4$$

where SW_{in} and SW_{out} are the incoming and outgoing shortwave radiations, respectively, and LW_{in} and LW_{out} are the incoming and outgoing longwave radiations, respectively.

From equations 2-2 and 2-3, it is evident that soil moisture is a significant variable that controls the partitioning of incoming precipitation and radiation (evaporation terms E and λE in both equations). Figure 2-1 provides an illustration of partitioning of the precipitation and radiation in the water balance and energy balance equations, respectively.

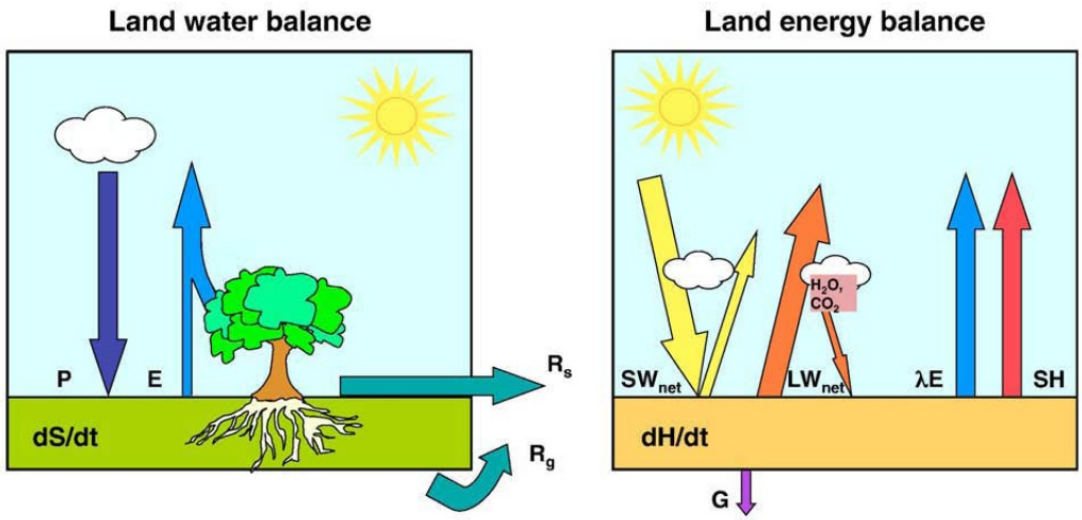

Figure 2-1: Schematic of the land water (left) and energy (right) balance for a given soil layer. (Adapted from (Seneviratne et al., 2010)).

The classical conceptual framework in Figure 2-2 describes the role of soil moisture in controlling evapotranspiration in soil moisture-limited regimes (Koster et al., 2004; Seneviratne et al., 2010).

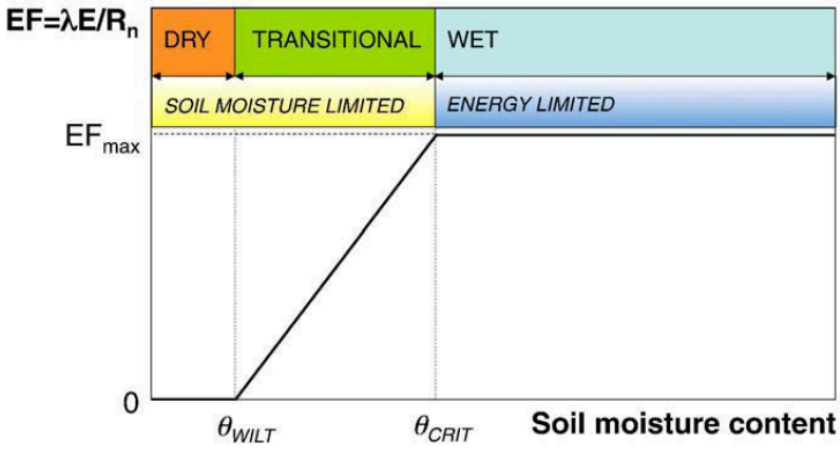

Figure 2-2: Soil moisture regimes and corresponding evapotranspiration regimes (Adapted from (Seneviratne et al., 2010)).

Two evapotranspiration regimes are defined (soil moisture-limited and energy-limited) and are characterized by the evaporative fraction, which can be expressed as:

$$EF = \frac{\lambda E}{R_n} \quad 2\text{-}5$$

The evaporation fraction is independent of soil moisture (i.e., not controlled by soil moisture) in the energy-limited regime when the soil moisture content is above the critical value θ_{CRIT}. In the dry region where the soil moisture content is below the wilting point (θ_{WILT}), no evaporation takes place. Hence, soil moisture is a first order constraint on evapotranspiration in the transitional climate regime where $\theta_{WILT} \leq \theta \leq \theta_{CRIT}$ (Koster et al., 2004; Seneviratne et al., 2006).

2.2 NASA Aquarius Satellite

The NASA Aquarius (Le Vine et al., 2007) instrument is a part of Aquarius/Satéllite de Aplicaciones Científicas (SAC-D), which was launched in June 2011 to measure sea surface salinity from space. The mission is a collaboration between NASA and Argentina's space agency, Comisión Nacional de Actividades Espaciales (CONAE), with participation from Brazil, Canada, France, and Italy. The Aquarius instrument, which was developed by NASA, is a combined active/passive microwave instrument that provides L-band (1.4 GHz) Tb observations.

The primary science objective of the Aquarius mission is to capture seasonal and annual sea surface salinity (SSS) anomalies using the combined active/passive microwave radiometer assembly. However, the study presented here utilizes the same sensor in soil moisture-related studies. The passive radiometers measure Tb at 1.413 GHz with both horizontal and vertical polarizations. At horizontal polarization, the sensitivity of soil emissivity to the soil moisture state is greater than at vertical polarization. On the other hand, at vertical polarization, the sensitivity to surface temperature is greater (Owe et al., 2001).

The radiometers provide three beams of Tb observations with a spatial resolution of 76 x 94 km, 84 x 120 km, and 96 x 156 km, respectively, which are pointed away from the sun to avoid glint. The active scatterometer additionally measures the backscatter from the surface, enabling a surface roughness correction during data processing.

2.3 L-band Radiative Transfer Model

The RTM used in this study is the zero-order, tau-omega RTM. This particular RTM is coupled with the GEOS-5 Catchment Land Surface Model (Catchment) (Koster et al., 2000) and ultimately provides L-band Tb predictions as a function of land surface inputs from the Catchment model on a 36-km Equal Area Scalable Earth (EASE) grid cell. The inputs to the RTM derived from Catchment are soil moisture, soil temperature, vegetation water content, and reference-level ($\sim$2 m) air temperature. The Tb estimates are obtained at both horizontal and vertical polarization (De Lannoy et al., 2013). The Tb at the top of the vegetation and atmosphere are expressed as:

$$Tb_{TOV,p} = T_s(1 - r_p)A_p + T_c(1 - \omega_p)(1 - A_p)(1 + r_p A_p) + Tb_{ad,p} r_p A_p^2 \quad 2\text{-}6$$

$$Tb_{TOA,p} = Tb_{au,p} + \exp(-\tau_{atm,p}) Tb_{TOV,p} \quad 2\text{-}7$$

where $Tb_{TOV,p}$ and $Tb_{TOA,p}$ are the top of the vegetation and atmosphere Tb [K] at polarization $p = (H, V)$ respectively, T_s and T_c are the surface soil (i.e., upper few centimeters) temperature [K] and canopy temperature [K] respectively, $Tb_{ad,p}$ and $Tb_{au,p}$ are the downward and upward atmospheric radiation [K] (Pellarin et al., 2003), A_p is the vegetation attenuation [-], $\exp(-\tau_{atm,p})$ is the atmospheric attenuation [-] (Pellarin et al., 2003), $\tau_{atm,p}$ is the atmospheric optical depth [-], r_p is the rough surface reflectivity [-], and ω_p is the scattering albedo [-].

The rough surface reflectivity is defined as:

$$r_p = \left[QR_q + (1-Q)R_p\right] \exp(-h) \cos^{\mathrm{Nr_p}}(\theta) \qquad 2\text{-}8$$

where Q [-] is the polarization mixing ratio, R_p [-] is the smooth surface reflectivity (Choudhury et al., 1979; Wang and Choudhury, 1981), h [-] is the roughness parameter that accounts for dielectric properties of the soil, and $\mathrm{N_{rp}}$ [-] is the angular dependence where $q = V$ for $p = H$ and (vice versa). The vegetation attenuation A_p [-] is given by (Jackson and Schmugge, 1991) a vegetation opacity model as:

$$A_p = \exp\left(-\frac{\tau_p}{cos(\theta)}\right) \qquad 2\text{-}9$$

where,

$$\tau_p = b_p * VWC = b_p * LEWT * LAI \qquad 2\text{-}10$$

τ_p [-] is the nadir vegetation opacity, b_p [-] is the vegetation structure parameter, VWC [kg m^{-2}] is the vegetation water content, $LEWT$(kg m^{-2}) is the leaf equivalent water thickness, and LAI [m^2 m^{-2}] is the leaf area index. The parameters for this RTM were calibrated using Soil Moisture Ocean Salinity (SMOS) (Kerr et al., 2010) observations for eventual use in estimating Aquarius observations.

2.4 ESA SMOS Satellite Mission

The Soil Moisture Ocean Salinity (SMOS) mission (Kerr et al., 2010, 2001) is one of the first major satellite missions to specifically map soil moisture (Leroux et al., 2014) and sea surface salinity from a space-based platform. Realizing the significance of surface soil moisture and sea surface salinity in the global water cycle and energy budget, it was launched in November 2009 by the European Space Agency (ESA). It also uses the principle of a low frequency (i.e., L-band) radiometer to obtain upwelling microwave

emissions from the surface with reduced perturbations associated with overlying vegetation. It carries an L-band radiometer that provides multi-angular, dual polarized (i.e., horizontal and vertical polarization) Tb observations at 50 km spatial resolution with a repeat interval of 3 days and a root mean squared error of 0.043 m^3 m^{-3} (Leroux et al., 2014).

The science objectives of the SMOS mission include better understanding of the global water cycle by monitoring surface soil moisture and ocean salinity and their subsequent contribution to global climate change by altering evaporation and precipitation flux. Monitoring ocean salinity will also allow scientists to better understand the global ocean circulation, the role of freshwater precipitation lenses, and other freshwater fluxes on salinity in the ocean and in the El-Niño Southern Oscillation (ENSO) (Kerr et al., 2010; Lukas and Lindstrom, 1991). Another objective of the mission is to estimate the root zone soil moisture that is biologically available to plants. Root zone soil moisture is correlated with surface soil moisture (Calvet et al., 1998) and is an important metric to estimate plant growth, transpiration, and photosynthetic activity from plants as well as impacts on short-term meteorologic forecasting (Calvet et al., 1998).

SMOS soil moisture retrieval performance was evaluated using in situ measurements from the Soil Climate Analysis Network (Schaefer et al., 2007) measurements (Al Bitar et al., 2012) which showed a reasonable agreement in capturing soil moisture dynamics but that SMOS-derived soil moisture was underestimated. However, a newer version of the soil moisture product provides a significant improvement (Leroux et al., 2014). Several other studies (Jackson et al., 2012; Leroux et al., 2014) also show the root mean squared error (RMSE) obtained from the SMOS

validation studies are within an acceptable range (Jackson et al., 2012) and better agree with ground-based measurements (Leroux et al., 2013).

2.5 SMAP Mission

The Soil Moisture Active Passive (SMAP) mission is an upcoming satellite mission that is intended to provide L-band active and passive (radar and radiometer) soil moisture observations from space, which is scheduled to be launched in October 2014 (Fang and Lakshmi, 2013). One of the key features of this mission is the observation of soil moisture and freeze/thaw state of the land surface that will help better represent water, energy, and carbon exchanges between the land and atmosphere (Entekhabi et al., 2010). The combined active and passive instrument will be used to integrate both high resolution and low accuracy backscattered data from the active radar in conjunction with low resolution and high accuracy observations from the passive radiometer in order to produce soil moisture products at 10-km resolution and freeze/thaw state at 3 km resolution. Objectives of the SMAP mission include better understanding of the linkages among water, energy and carbon cycles. The overarching goal of SMAP is to develop better skill in climate, flood, drought and weather forecasting.

2.6 Implications of Climate Variability on Soil Moisture

Several studies have been conducted to study climate variations associated with soil moisture variability. Thornthwaite (1948) discussed the role of potential evapotranspiration as a climate factor. Certain regions of the world show substantial precipitation anomalies associated with soil moisture variability due to enhanced land-atmosphere interactions. The Global Land Atmosphere Coupling Experiment (GLACE) (Guo et al., 2006; Koster et al., 2006) show that “hot-spots” exist where precipitation is

governed by soil moisture (Koster et al., 2004). Such regions are generally located in transitional climate zones that lie between wet and dry climates where evaporation is controlled by soil moisture. Lawrence and Hornberger (2007) investigated soil moisture variability across climate zones, which largely explained the variance in measured soil moisture content.

The United States consists of several climate zones based on Köppen Climate Classifications (Koppen, 1936). The Köppen Climate Classification system is one of the most widely used climate classification systems which defines climate zones on the basis of vegetation in conjunction with seasonal temperature and precipitation patterns (McKnight and Hess, 2000). Study areas were selected on the basis of major climate zones in the continental United States in order to evaluate the RTM performances relative to Aquarius observations. Details of the study areas with their climate zones characteristics are described in the following chapter (Section 3.2.2).

Chapter 3: Data and Methodology

3.1 General

The objective of this study is to evaluate the RTM-predicted Tb when compared to the Aquarius Tb observations. Since Tb is a function of soil emissivity, which changes with soil moisture content, its variability will result in Tb variability. However, other factors such as soil roughness and overlying vegetation play a significant role in Tb retrieval from sensors and model estimates. This chapter includes details of the study area and their selection, the data used for this study, and the methodology used in the study.

3.2 Study Areas

The study sites were selected based on USCRN (Bell et al., 2013) station locations distributed across the continental United States in different climate regions as defined by Köppen Climate Classification. There are 114 USCRN observation stations across the contiguous US (Palecki and Bell, 2013) among which 33 stations were selected based on geolocation with Aquarius satellite orbit tracks (Figure 3-1). The study period spans from 25 August 2011 to 31 October 2013 based on availability of processed data from both Aquarius and the RTM.

3.2.1 Study Location List

The USCRN stations are identified by Weather Bureau Army Navy (WBAN) numbers. The full list of the study locations is provided in Table 3-1 and shown in *Figure 3-1*.

Table 3-1: Selected study locations alphabetized by state.

WBAN	Name	Location	State	Latitude	Longitude
63858	Auburn University, Black Belt Research and Extension Center	Selma	AL	32.4567	-87.2422
53131	Sonora Desert Museum	Tucson	AZ	32.2395	-111.1696
93245	University of California - Davis (Bodega Marine Laboratory)	Bodega	CA	38.32085	-123.07458
53151	San Diego State Univ's Santa Margarita Ecological Reserve (Old Mine Road)	Fallbrook	CA	33.4392	-117.1904
93243	Kesterson Reservoir (US Bureau of Reclamation)	Merced	CA	37.2381	-120.8825
53139	Death Valley National Park (Stovepipe Wells Site)	Stovepipe Wells	CA	36.602	-117.1449
53150	Yosemite National Park, (Crane Flat Lookout)	Yosemite Village	CA	37.75918	-119.82073
3061	Mesa Verde National Park (Far View Site)	Cortez	CO	37.2553	-108.5035
3063	USDA Comanche National Grassland	La Junta	CO	37.8639	-103.8224
94074	Ag. Res. Svc. Central Plains Exp. Range (SGS LTER at CSU)	Nunn	CO	40.8066	-104.7552
92826	Big Cypress National Preserve (Ochopee Headquarters Vista Site)	Everglades City	FL	25.8996	-81.3183
63850	USDA/ARS Watkinsville (Colham Ferry Site)	Watkinsville	GA	33.7837	-83.3896
54811	Northern Illinois Agronomy Research Center	Shabbona	IL	41.843	-88.8513
63849	Mammoth Cave National Park (Job Corps Site)	Bowling Green	KY	37.2504	-86.2325
63838	University of Kentucky (Woodford County Site)	Versailles	KY	38.0945	-84.7465
53961	Ouachita National Wildlife Refuge	Monroe	LA	32.8833	-92.1165
94644	University of Maine (Rogers Farm Site)	Old Town	ME	44.9281	-68.7006
4994	Agassiz National Wildlife Refuge (Maintenance Shop Site)	Goodridge	MN	48.3055	-95.8744

23908	Shawnee Trail Conservation Area	Joplin	MO	37.4273	-94.588
23909	White River Trace Conservation Area (Stand 4, Compartment 7)	Salem	MO	37.6334	-91.72263
4130	Glacier National Park (St. Mary Site)	St. Mary	MT	48.7412	-113.433
4139	Sheldon National Wildlife Refuge, (Little Sheldon Site)	Denio	NV	41.84834	-119.6357
53136	Nevada Test Site (Desert Rock Meteorological Lab)	Mercury	NV	36.624	-116.0225
54851	North Appalachian Experimental Watershed (CRN site)	Coshocton	OH	40.3667	-81.7829
3055	OK Panhandle Research & Extn. Center (Native Grassland Site)	Goodwell	OK	36.5993	-101.595
53182	Oklahoma Panhandle State Univ., School of Agriculture (Permanent Pasture)	Goodwell	OK	36.56828	-101.60915
4125	John Day Fossil Beds Nat'l. Mon.(Sheep Rock Hdqs.)	John Day	OR	44.556	-119.6459
63826	Clemson University (Edisto Research & Edu. Ctr.)	Blackville	GA	33.355	-81.3279
94081	SDSU Antelope Research Station (Calving Pasture Site)	Buffalo	SD	45.516	-103.3017
3054	Muleshoe National Wildlife Refuge (Headquarters Site)	Muleshoe	TX	33.9557	-102.774
22016	Big Bend National Park	Panther Junction	TX	29.33	-103.2
4138	Golden Spike National Historic Site (Visitor Center Site)	Brigham City	UT	41.61652	-112.54567
4223	North Cascades National Park (Marblemount)	Darrington	WA	48.5405	-121.446

3.2.2 Key Characteristics of the Climate Classes

The climate classes in the continental US range from cold/humid subtropical to semi-arid (Figure 3-1) based on the criteria described in Peel et al. (2007). Different types of climate classes in the continental US are described below as defined in Peel et al. (2007).

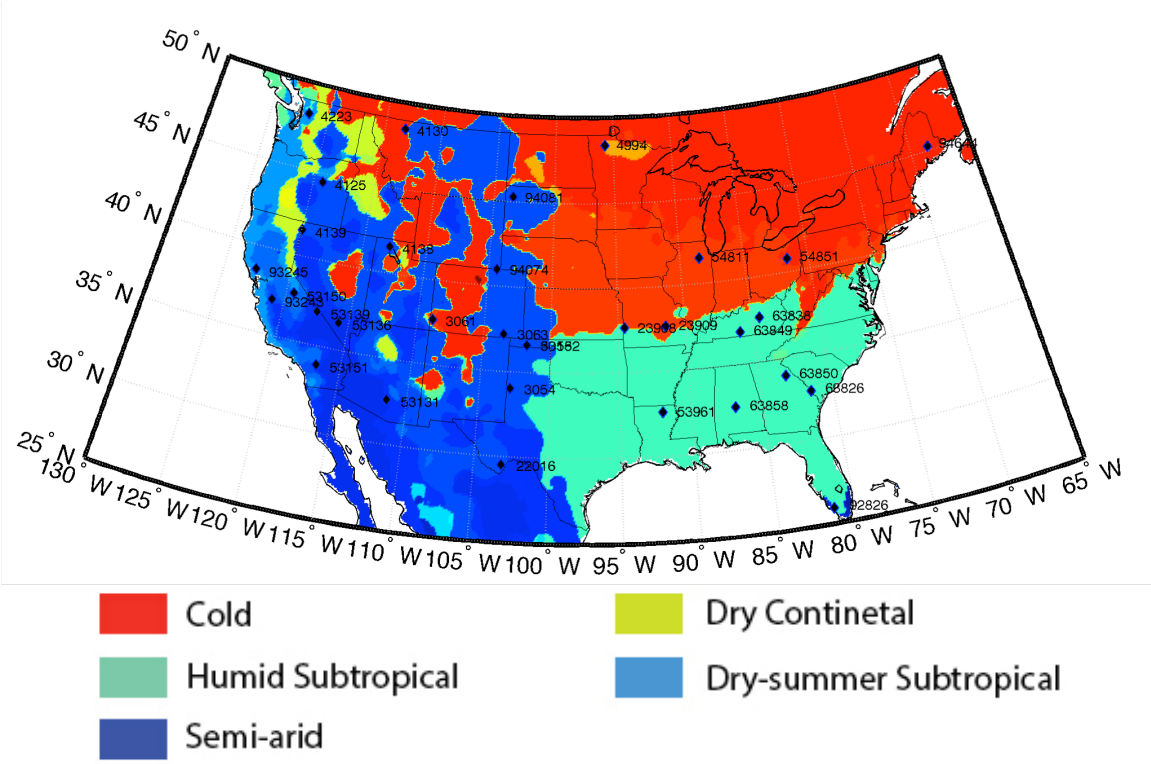

Figure 3-1: Map of the study area with climate classes.

Humid Continental/Cold Climate: This climate is characterized by cold winter and hot/warm summer, which is a dominant climate type in the continental US. Based on the summer time temperatures, this climate type is further divided into hot summer and warm summer type. The hot summer continental climate is generally found in high 30s and low 40s latitude whereas warm summer condition is found in the high 40s and low 50s latitude in North America. In this region, there is a substantial amount of precipitation during all seasons, which is a key feature in this class. Further, it is

classified according to the temperature pattern. During the hottest month the temperature rises above 22^{o}C in the hot summer climate and the temperature is above 10^{o}C for at least 4 months during the warm summer climate.

Dry Continental Climate: This climate is characterized by cold climate with a dry summer where precipitation is less than 40 mm in the driest month. Further, it is classified according to the temperature in the hottest month below 22^{o}C as well as at least four months of temperature above 10^{o}C.

Humid Subtropical Climate: This is a temperate climate zone with a temperature greater than 22^{o}C in the hottest month and between 0^{o}C to 18^{o}C during the coldest month and with a significant amount of precipitation during all seasons.

Dry-summer Subtropical Climate: This climate class is almost similar to the humid subtropical climate except for less than 40 mm of precipitation as well as less than one-third of the precipitation in the wettest winter month.

Cold Semi-arid/Steppe Climate: This climate is characterized by hot and dry summers when the mean annual precipitation is less than a threshold value based on potential evapotranspiration. If the mean annual temperature is less than 18^{o}C then it is classified as cold semi-arid climate.

3.3 Data Sets

3.3.1 USCRN Data

The USCRN stations are established, maintained, and operated by the National Oceanic and Atmospheric Administration (NOAA) to provide reference information about climate change in the United States (Heim, 2001; Palecki and Bell, 2013). Among other climate data, the USCRN stations provide direct measurement of hourly in situ

volumetric soil moisture as well as air temperature and precipitation data at 114 locations across the contiguous United States. The USCRN data used for this study include hourly data of air temperature [^{o}C], precipitation [mm/hr], shortwave flux [W/m^{2}] and volumetric soil moisture [m^{3}/m^{3}] data at depths of 5, 10, 20, 50, 100 cm. To be consistent with the passive microwave data from Aquarius, only volumetric soil moisture time series data from 5 cm depth are compared to Aquarius Tb.

3.3.2 Aquarius Brightness Temperature

Data used in the study include the Level-2 (single orbit) product of Aquarius Tb processed by the NASA Jet Propulsion Laboratory (JPL) in Hierarchical Data Format (HDF5). Three radiometers onboard observe emitted energy from the Earth's surface and provides Tb observations from three different beams. The beam incident angles are 29.36, 38.49 and 46.29 degrees with a ground footprint of 76 x 94 km, 84 x 120 km and 96 x 156 km, respectively (Figure 3-2). Aquarius is a polar-orbiting satellite that covers the entire globe with a repeat interval of 7 days (Le Vine et al., 2007).

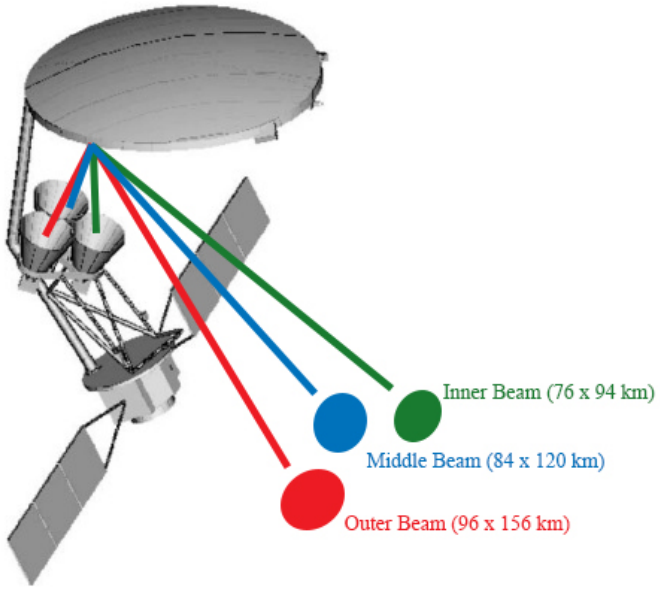

Figure 3-2: Illustration of Aquarius footprint (reproduced from (Koblinsky et al., 2003)).

Aquarius Level-2 data include Tb observations for an individual orbit (both ascending and descending) in both horizontal and vertical polarizations. Figure 3-3 shows processed Tb observation for a single day, which is an agglomeration of multiple ascending and descending orbits.

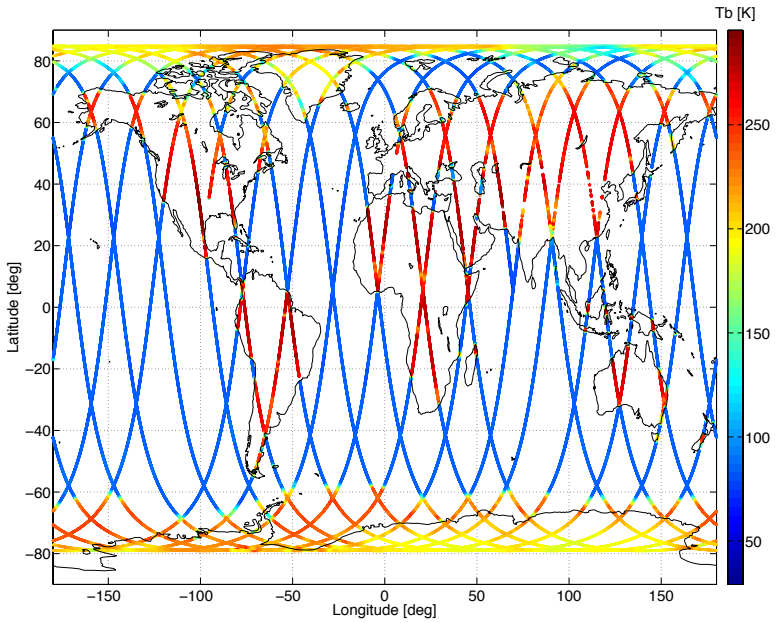

Figure 3-3: Single day worldwide Tb [K] observation from Aquarius.

The Aquarius Tb retrieval follows the principle of passive microwave radiometry for soil moisture as described in Jackson and Schmugge (1989). The Tb is defined as (Jackson and Schmugge, 1989):

$$Tb = \tau\left[(1 - e_v)T_{sky} + e_v T_{surf}\right] + T_{atm} \qquad 3\text{-}1$$

where τ is the atmospheric transmissivity [-], e_v is the vegetation emissivity [-], T_{sky} is the reflected sky brightness [K], T_{surf} is the thermal temperature of the surface [K] and T_{atm} is the direct atmospheric contribution [K]. Further, e_v is defined as

$$e_v = 1 + \left(e_{surf} - 1\right)\exp\left(b * W\right) \qquad 3\text{-}2$$

where, e_v is the rough surface emissivity [-], b is the vegetation attenuation parameter [-], and W is the vegetation water content [m^3/m^3]. e_{surf} [-] is a function of soil emissivity e_{soil} [-] and is defined as:

$$e_{surf} = 1 + (e_{soil} - 1)\exp(h) \quad 3\text{-}3$$

where h [-] is the surface roughness parameter. e_{soil} [-] is a function of the complex dielectric constant of the soil and is given by,

$$e_{soil} = 1 - \left|\frac{(\sqrt{k} - 1)}{\sqrt{k} + 1}\right|^2 \quad 3\text{-}4$$

where k is the complex dielectric constant [-].

3.3.3 L-band Radiative Transfer Model Data

The Tb estimates are obtained from the GEOS-5 L-band radiative transfer model (Section 2.3). The RTM parameters are calibrated against SMOS observations (De Lannoy et al., 2013) using multiple incident angles and horizontal and vertical polarizations in order to produce an unbiased estimate of Tb.

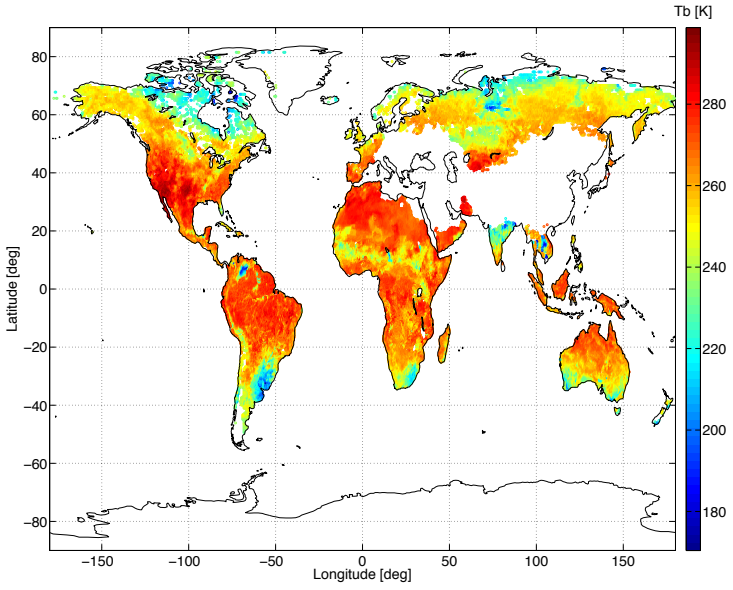

Figure 3-4: Tb [K] prediction from L-band RTM on 25 August, 2011 at 00:00 hours

This RTM is processed so that it provides a prediction of Tb every three hours. However, microwave signals from the surface are highly prone to be contaminated by radio frequency interference (RFI) from a variety of transmitters used for communication, especially from low frequency radiometers (Li et al., 2004; Njoku et al., 2005). A large area in Europe and Asia were masked out during quality control because of strong RFI contamination. Moreover, during calibration of the RTM from SMOS observations, frozen soil conditions were neglected (De Lannoy et al., 2013) due to improper model physics when soil moisture is solid rather than liquid (Montzka et al., 2013). Further, extensive quality control (De Lannoy et al., 2013) of the SMOS observations were also applied to places near water bodies, during intensive precipitation events (greater than 10 mm/h), freezing soil conditions (temperature below 273.4 K), and in the presence of snow (snow water equivalent greater than 10^{-4} kg/m^2). As a result, Tb predictions at many locations on globe were masked.

3.4 Methodology

Measurements from Aquarius were collected from locations that were within 0.5 degrees from the selected USCRN stations. A second geolocation constraint was added such that study locations were selected when the Aquarius overpass crossing-point of both ascending and descending orbits was within 0.5 degrees the USCRN stations. The latter search criteria was implemented in order to maximize the number of Aquarius observations for use during the statistical analysis.

3.4.1 Algorithm

The following algorithm was used for the study:

1. Select a location

2. Set start date, finish date, distance, and temporal threshold
3. Define polarization (horizontal or vertical)
4. Set current time = start time
5. Check if current time ≤ finish time. If yes, continue to step 6; otherwise go to step 15
6. Load Aquarius and RTM files
7. Get Tb observations from Aquarius and Tb predictions from the RTM
8. Find Aquarius observations and RTM predictions within 0.5-degree spatial threshold
9. Store observations and predictions into their respective vectors
10. Increment to next time step, go to step 5
11. Find observations and predictions within temporal threshold of 1.5 hours
12. Calculate statistics
13. Conduct seasonal analysis
14. Start a new location and go to step 1

This algorithm is illustrated using a flowchart in Figure 3-5.

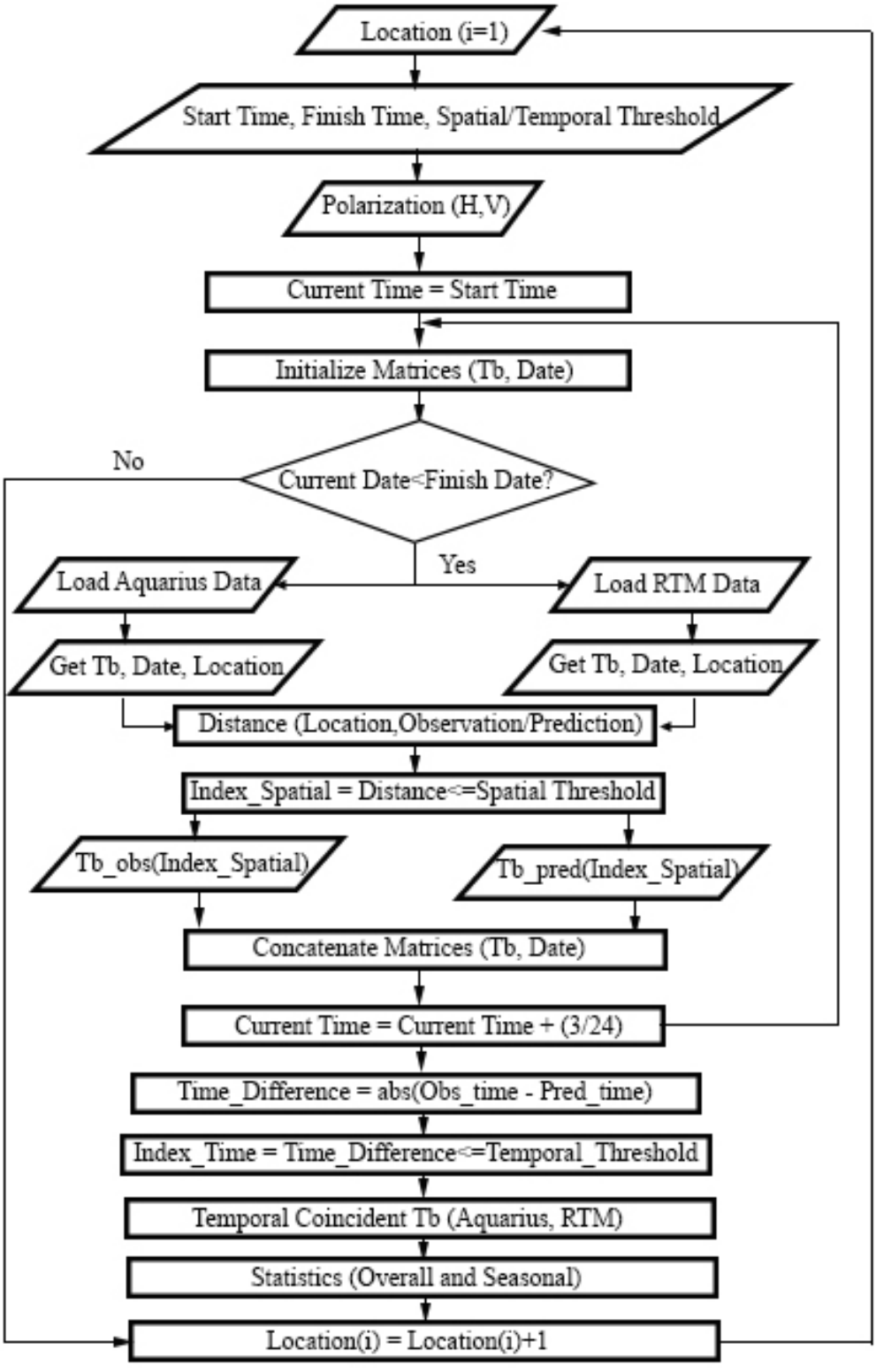

Figure 3-5: Flowchart illustrating the methodology of the study

3.4.2 Analysis and Statistics

Statistics are calculated from the Aquarius Tb observations and the RTM Tb predictions between the study period from 25 August 2011 to 31 October 2013. Statistics are the correlation coefficient, R [-], the bias [K] and the root mean squared error (RMSE) [K] (a.k.a. standard error of estimate, S_e), which are given by,

$$R = \frac{\mathrm{cov}\left(Tb_{pred}, Tb_{obs}\right)}{\sigma_{Tb_{pred}}\sigma_{Tb_{obs}}} \tag{3-5}$$

$$bias = \frac{1}{n}\sum_{i=1}^{n}\left(Tb_{pred,i} - Tb_{obs,i}\right) \tag{3-6}$$

and

$$S_e = RMSE = \sqrt{\frac{1}{n}\sum_{i=1}^{n}\left(Tb_{pred,i} - Tb_{obs,i}\right)^2} \tag{3-7}$$

where $\mathrm{cov}(.)$ is the covariance operator, Tb_{pred} is the predicted Tb [K] simulated by the RTM, Tb_{obs} is the observed Tb [K] by the Aquarius instrument, σ [K] is the standard deviation of the observed or predicted Tb, and n is the number of nonzero Tb values. The correlation coefficient, R, provides the degree of linear association between the variables and is used as a measure of accuracy (Ayyub and McCuen, 2011). The bias is a measure of systematic error variation where a positive value indicates the model overpredicts the observation whereas a negative value indicates the model underpredicts the observations. The standard error of estimate or RMSE represents both systematic (bias) and nonsystematic errors. It is also a measure of accuracy that indicate the extent of spread of the predictions around the observation.

Seasonal variations in the observed and predicted Tb in the study area are also evaluated. Different climatic regions are characterized by precipitation patterns and temperature anomalies, which dictate seasonal soil moisture variation (Hong and Pan, 2000) at a local scale. Tb data were segregated for each of the distinct seasons in the United States, namely, winter (December, January, February), spring (March, April, May), summer (June, July, August) and fall (September, October, November). Moreover, time series of volumetric water content [m^3/m^3] are compared against the Aquarius time series in order to determine whether the Tb observations are consistent with the theoretical volumetric water content anomaly, which verifies their inversely proportional relationship.

Chapter 4: Results and Discussions

4.1 General

This chapter presents the results, relevant statistics, and discussions. First, comparisons at the study locations are presented with time series plots and tabular representation of statistics for the entire study period. Next, seasonal statistics over a given study period are presented. Finally, time series comparison of Aquarius Tb with USCRN near-surface volumetric soil moisture data are presented.

4.2 Evaluation of RTM

The NASA GEOS-5 RTM Tb is evaluated using the Aquarius Tb product. Climate characteristics on soil moisture variability are key to this study. For each of the climate classes, results are provided in the following subsections.

4.2.1 Statistics in Different Climate Regions

4.2.1.1 Humid Continental/Cold Climate

One of the key characteristics of this climate region is the precipitation amount throughout the year. This region is generally cold and humid with a substantial amount of precipitation distributed all the year round. Figure 4-1 and Figure 4-2 show the observed Aquarius and RTM time series for this climate class (horizontal polarization and vertical polarization, respectively). Statistics for both polarizations are listed in Table 4-1 and Table 4-2.

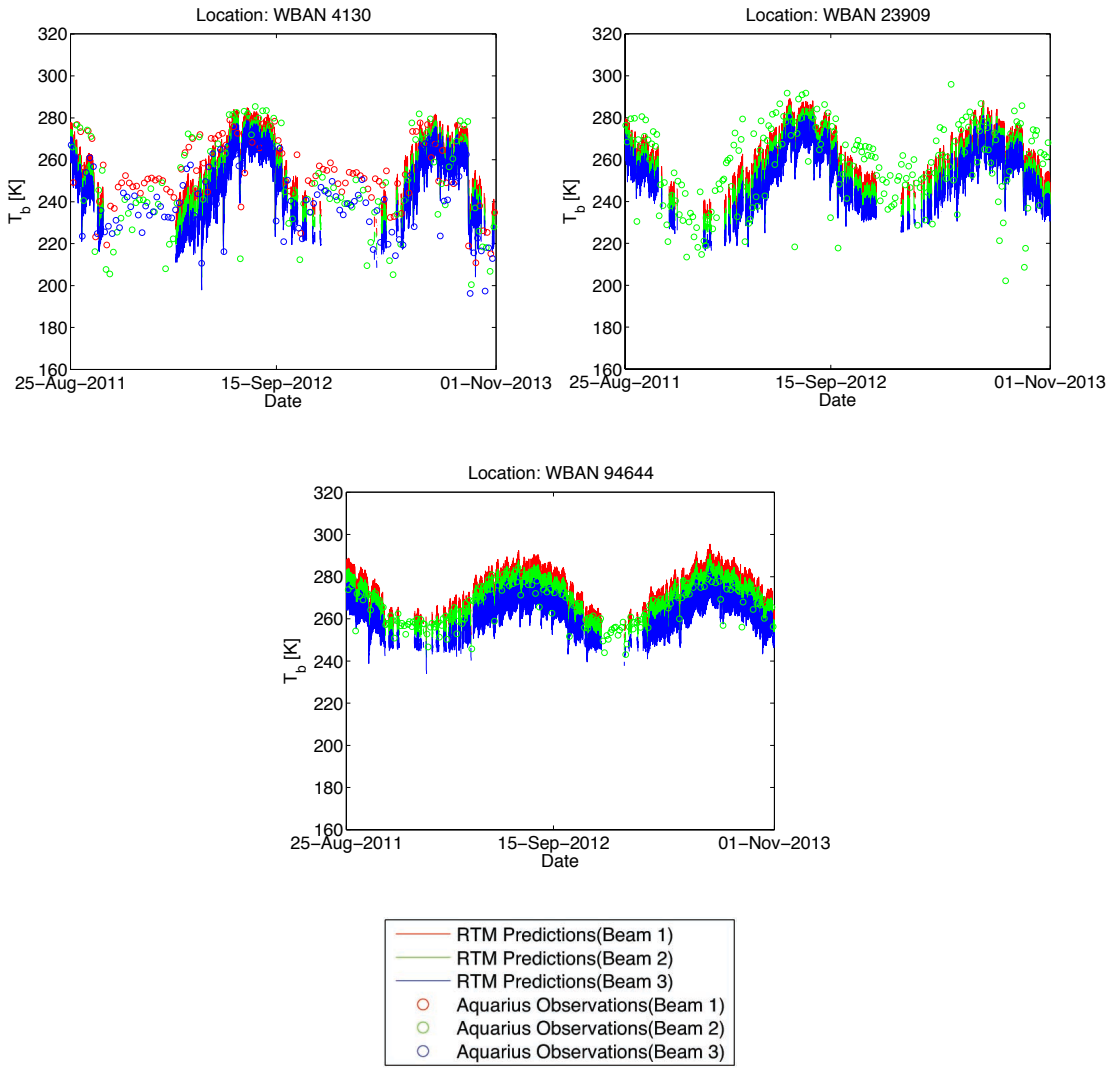

Figure 4-1: Time series plots for humid continental/cold climate (horizontal polarization)

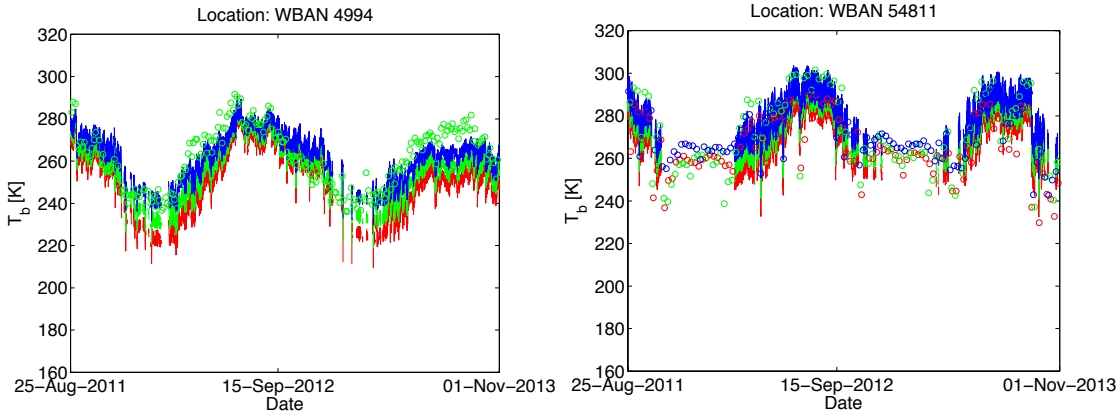

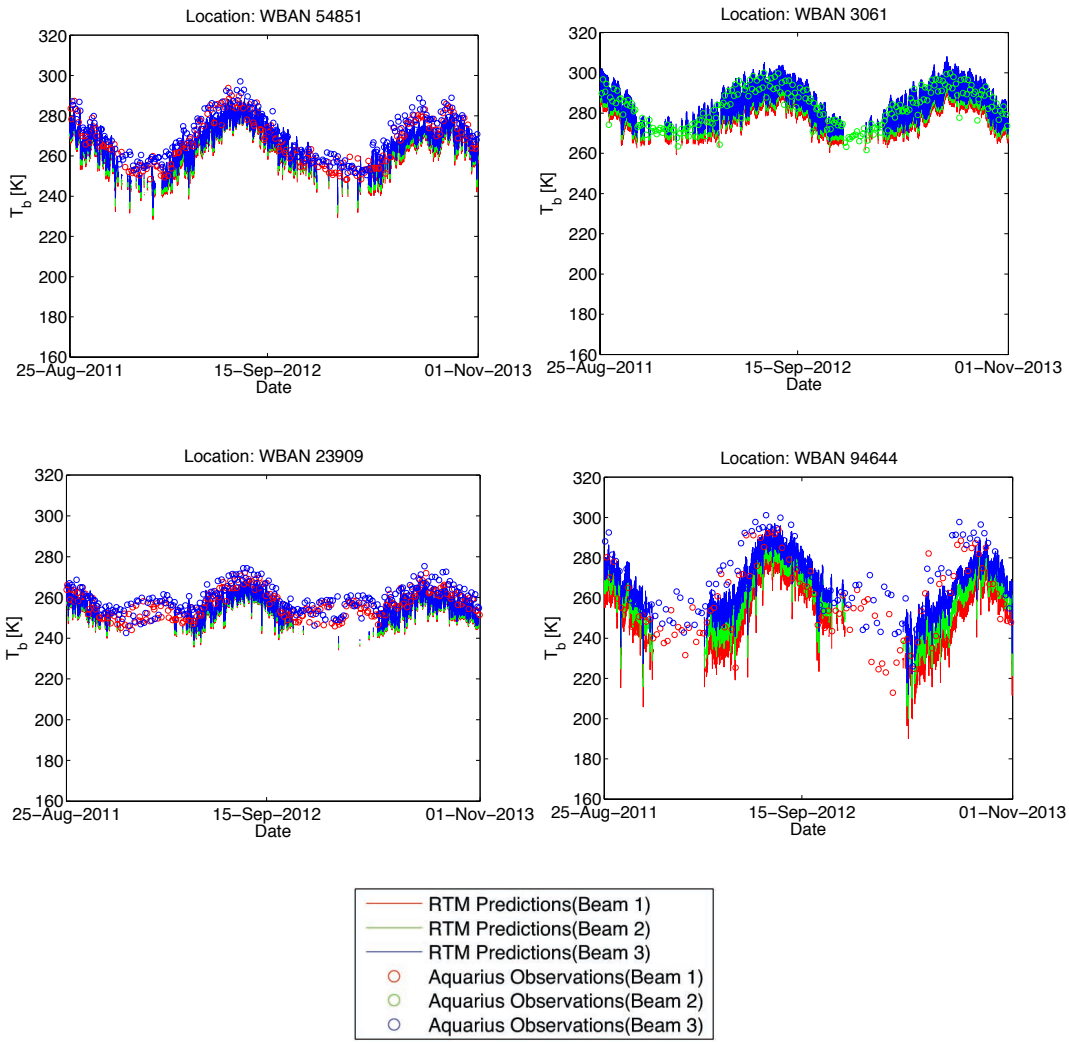

Figure 4-2: Time series plots for humid continental/cold climate (vertical polarization)

Figure 4-1 shows the time series in horizontal polarization. The locations WBAN 4130 (Glacier National Park, St. Mary, MT site) and 23909 (White River Trace Coservation Area, Salem, MO) show higher dynamics in both observed and predicted Tb than the other location (WBAN 94644, Unviersity of Maine, Old Town site). Statistics show (Table 4-1) higher uncertainty (i.e., standard deviations) at these sites. The presence of vegetation at the Glacier National Park may adversely influnce Tb retrieval in the L-band. The site 94644 shows a better agreement than the previous two sites, which is

reflected by the lower RMSE and a higher correlation coefficient. The presence of snow during the winter, however, limits the validity of the RTM predictions.

Figure 4-2 shows time series for vertical polarization in cold climate. Presence of snow is also evident here due the to unavailability of RTM predictions during winter. The sites 3061 (Mesa Verde National Park, CO), 54851 (North Appalachian Experimental Watershed, OH), and 23909 (White River Trace Coservation Area, Salem, MO) show a better agreement with the Aquarius in terms of correlation coefficient (Table 4-2).

Table 4-1: Statistics for humid continental/cold climate (horizontal polarization)

WBAN	Beam	Mean Tb [K]		Standard Deviation [K]		Bias [K]	RMSE [K]	R [-]
		Aquarius	RTM	Aquarius	RTM			
4130	1	254.3	255.6	15.7	14.2	9.3	14.9	0.67
	2	248.1	251.4	22.6	15.2	3.7	14.0	0.72
	3	241.6	246.8	17.1	16.5	6.9	14.2	0.75
23909	1	N/A	N/A	N/A	N/A	N/A	N/A	N/A
	2	257.5	256.0	19.3	12.8	7.8	16.3	0.63
	3	N/A	N/A	N/A	N/A	N/A	N/A	N/A
94644	1	N/A	N/A	N/A	N/A	N/A	N/A	N/A
	2	266.9	267.4	9.4	8.8	4.1	5.7	0.88
	3	N/A	N/A	N/A	N/A	N/A	N/A	N/A

N/A: Not Available (due to Aquarius measurements not falling within the spatial/temporal threshold)

Table 4-2: Statistics for humid continental/cold climate (vertical polarization)

WBAN	Beam	Mean [K]		Standard Deviation [K]		Bias [K]	RMSE [K]	R [-]
		Aquarius	RTM	Aquarius	RTM			
3061	1	N/A	N/A	N/A	N/A	N/A	N/A	N/A
	2	282.5	282.6	9.6	8.7	4.9	6.0	0.91
	3	N/A	N/A	N/A	N/A	N/A	N/A	N/A
4994	1	N/A	N/A	N/A	N/A	N/A	N/A	N/A
	2	260.9	257.3	14.1	13.1	7.9	11.4	0.79
	3	N/A	N/A	N/A	N/A	N/A	N/A	N/A
54811	1	265.4	270.8	13.7	12.2	5.6	10.8	0.70
	2	271.0	275.9	17.6	11.5	0.8	8.5	0.80
	3	271.5	280.7	12.5	10.5	3.3	7.3	0.84
54851	1	267.1	263.5	11.6	10.4	8.4	9.4	0.91
	2	N/A	N/A	N/A	N/A	N/A	N/A	N/A
	3	270.2	266.3	11.2	9.5	7.7	8.5	0.92
23909	1	256.5	253.9	6.5	5.9	5.5	6.1	0.91
	2	N/A	N/A	N/A	N/A	N/A	N/A	N/A
	3	259.5	255.7	6.4	5.6	7.5	7.7	0.94
94644	1	257.6	252.6	18.7	16.1	8.9	14.8	0.75
	2	N/A	N/A	N/A	N/A	N/A	N/A	N/A
	3	268.9	267.0	18.2	13.1	6.1	12.2	0.78

N/A = Not Available (due to Aquarius measurements do not fall within the spatial/temporal threshold)

4.2.1.2 Humid Subtropical Climate

This climate region is also characterized by substantial amounts of precipitation during all seasons, but with a higher summertime temperature than the humid continental climate. Time series (Figure 4-3 and Figure 4-4) and statistics (Table 4-3 and Table 4-4) for this climate are provided below:

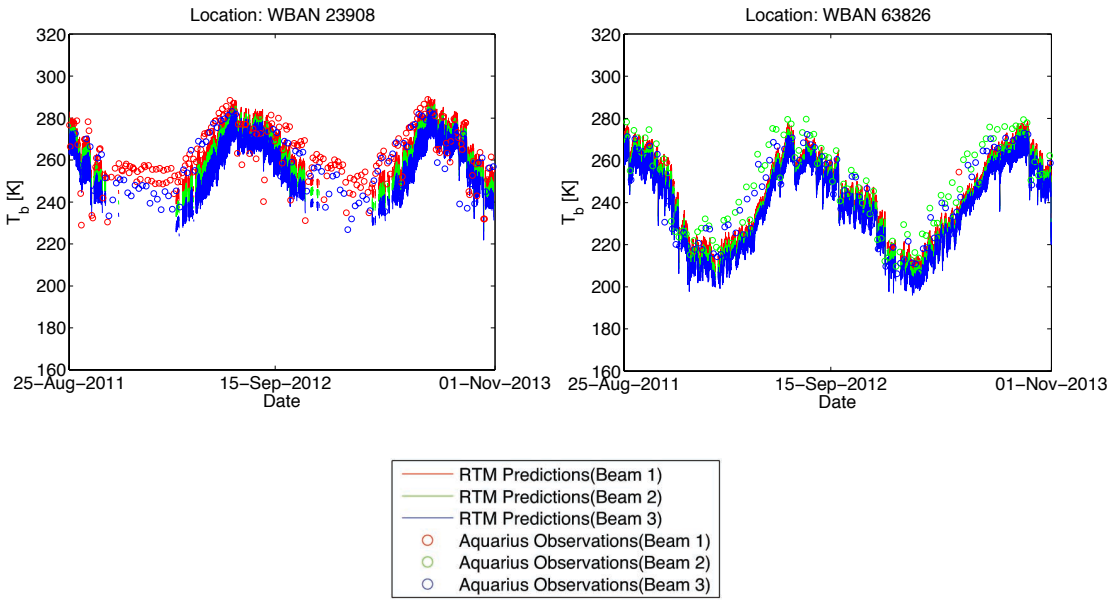

Figure 4-3: Time series plots for humid subtropical climate (horizontal polarization)

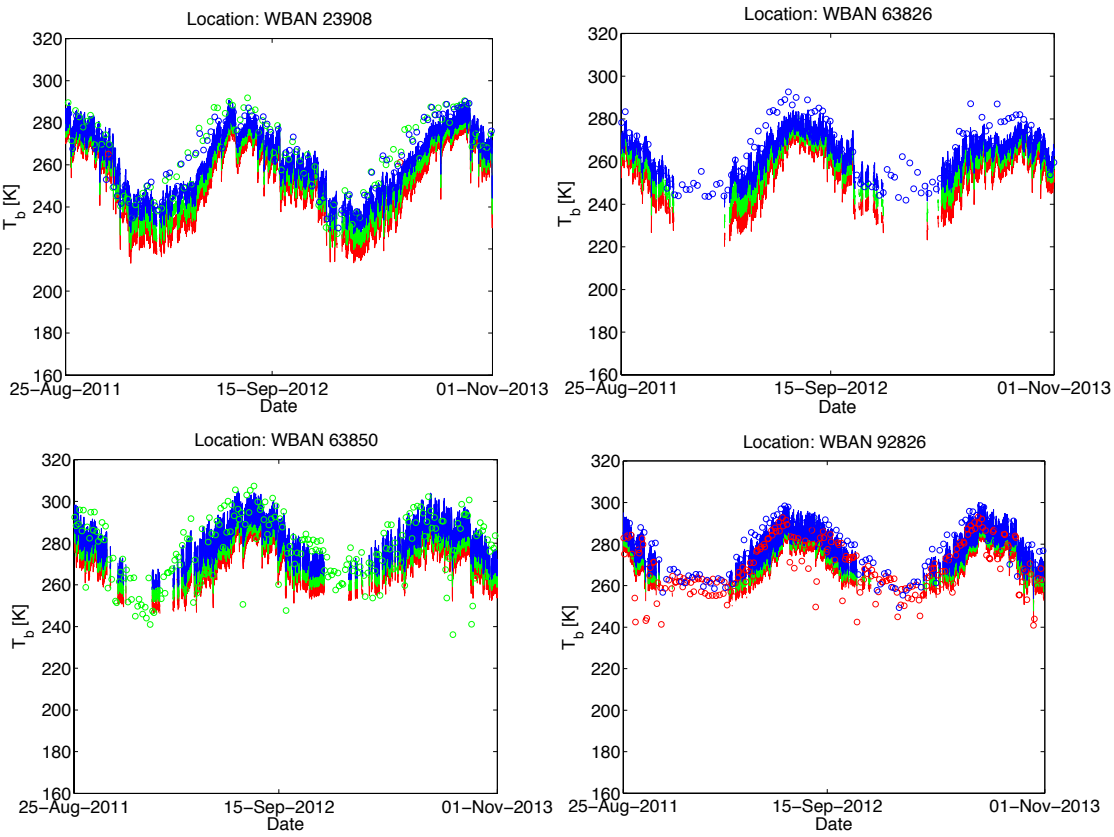

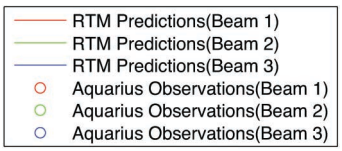

Figure 4-4: Time series plot for humid subtropical climate (vertical polarization)

From Figure 4-3, the site 23908 (Shawnee Trail Conservation Area, MO) has poor agreement with the measurement (Table 4-3), but smaller bias than the other site 63826 (Clemson University, Edisto Research and Education Center, GA). However, the later site has poorer statistics (higher bias and RMSE). For vertical polarization the site 63850 (USDA/ARS, GA) shows lower correlation than the other sites with a higher RMSE.

Table 4-3: Statistics for humid subtropical climate (horizontal polarization)

WBAN	Beam	Mean Tb [K]		Standard Deviation [K]		Bias [K]	RMSE [K]	R [-]
		Aquarius	RTM	Aquarius	RTM			
23908	1	262.2	265.0	13.2	10.8	3.0	9.9	0.67
	2	N/A	N/A	N/A	N/A	N/A	N/A	N/A
	3	257.9	257.5	14.3	12.6	4.5	10.7	0.70
63826	1	N/A	N/A	N/A	N/A	N/A	N/A	N/A
	2	248.8	239.9	20.3	19.6	7.3	10.9	0.91
	3	243.5	237.2	20.1	19.8	9.9	12.0	0.94

N/A: Not Available (due to Aquarius measurements not falling within the spatial/temporal threshold)

Table 4-4: Statistics for humid subtropical climate (vertical polarization)

WBAN	Beam	Mean Tb [K]		Standard Deviation [K]		Bias [K]	RMSE [K]	R [-]
		Aquarius	RTM	Aquarius	RTM			
23908	1	N/A	N/A	N/A	N/A	N/A	N/A	N/A
	2	265.0	255.6	17.6	17.1	7.5	11.1	0.89
	3	263.8	260.7	16.6	15.5	6.8	9.2	0.92
92826	1	268.8	273.5	12.1	9.5	1.1	8.1	0.70
	2	N/A	N/A	N/A	N/A	N/A	N/A	N/A
	3	276.8	279.4	12.6	8.6	0.1	4.7	0.86
63826	1	N/A	N/A	N/A	N/A	N/A	N/A	N/A
	2	N/A	N/A	N/A	N/A	N/A	N/A	N/A
	3	264.3	264.5	14.5	8.8	4.7	7.0	0.89
63850	1	N/A	N/A	N/A	N/A	N/A	N/A	N/A
	2	276.8	276.0	16.4	10.3	6.7	12.8	0.69
	3	N/A	N/A	N/A	N/A	N/A	N/A	N/A

N/A: Not Available (due to Aquarius measurements not falling within the spatial/temporal threshold)

4.2.1.3 Semi-Arid Climate

This climate region is dry during the summer with limited precipitation. The time series plot (Figure 4-5 and Figure 4-6) and statistics (Table 4-5 and Table 4-6) are provided below:

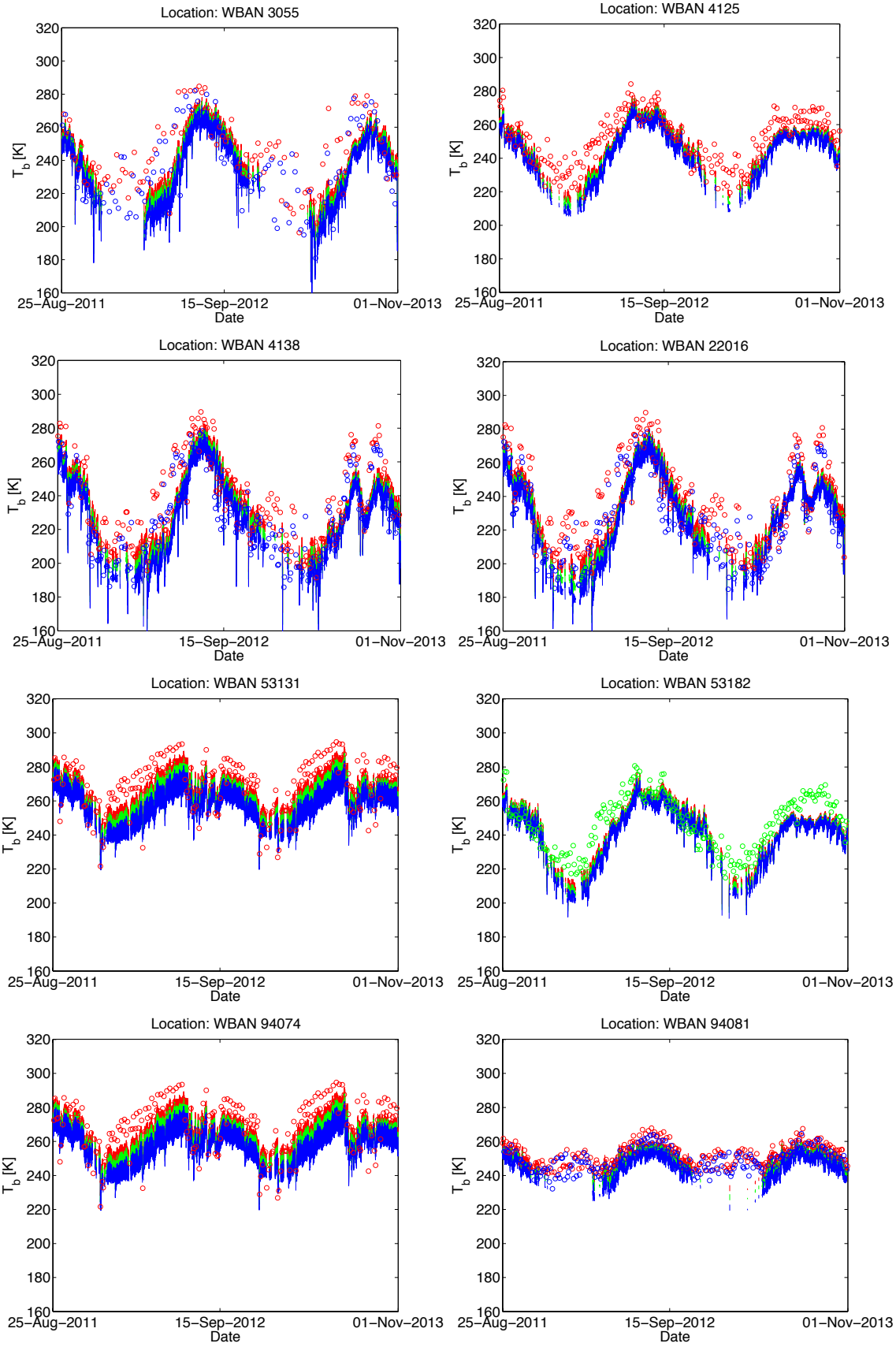
Location: WBAN 3055
Location: WBAN 4125
Location: WBAN 4138
Location: WBAN 22016
Location: WBAN 53131
Location: WBAN 53182
Location: WBAN 94074
Location: WBAN 94081
T_b [K]
320
300
280
260
240
220
200
180
160
25–Aug–2011
15–Sep–2012
01–Nov–2013
Date

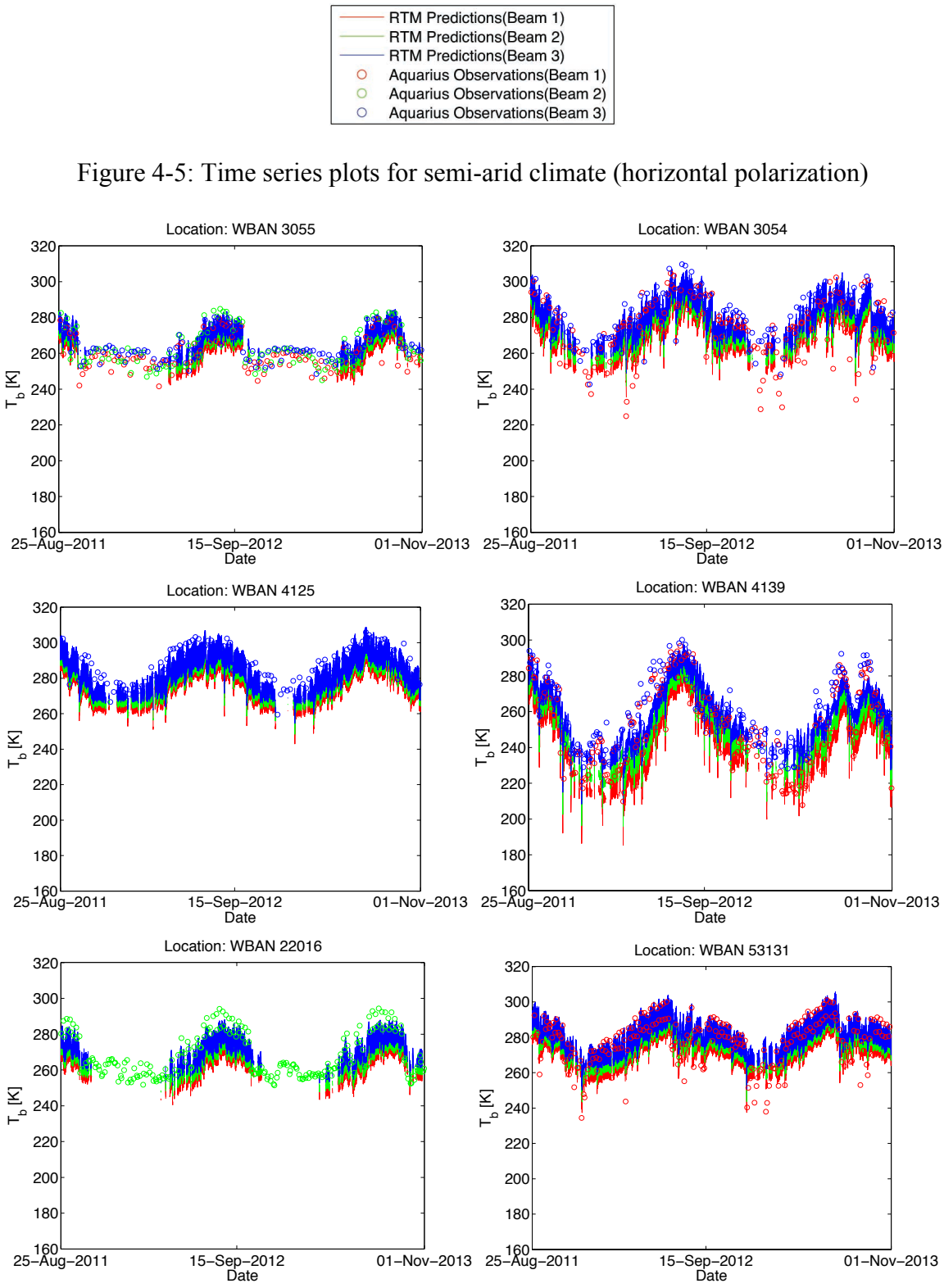

Figure 4-5: Time series plots for semi-arid climate (horizontal polarization)

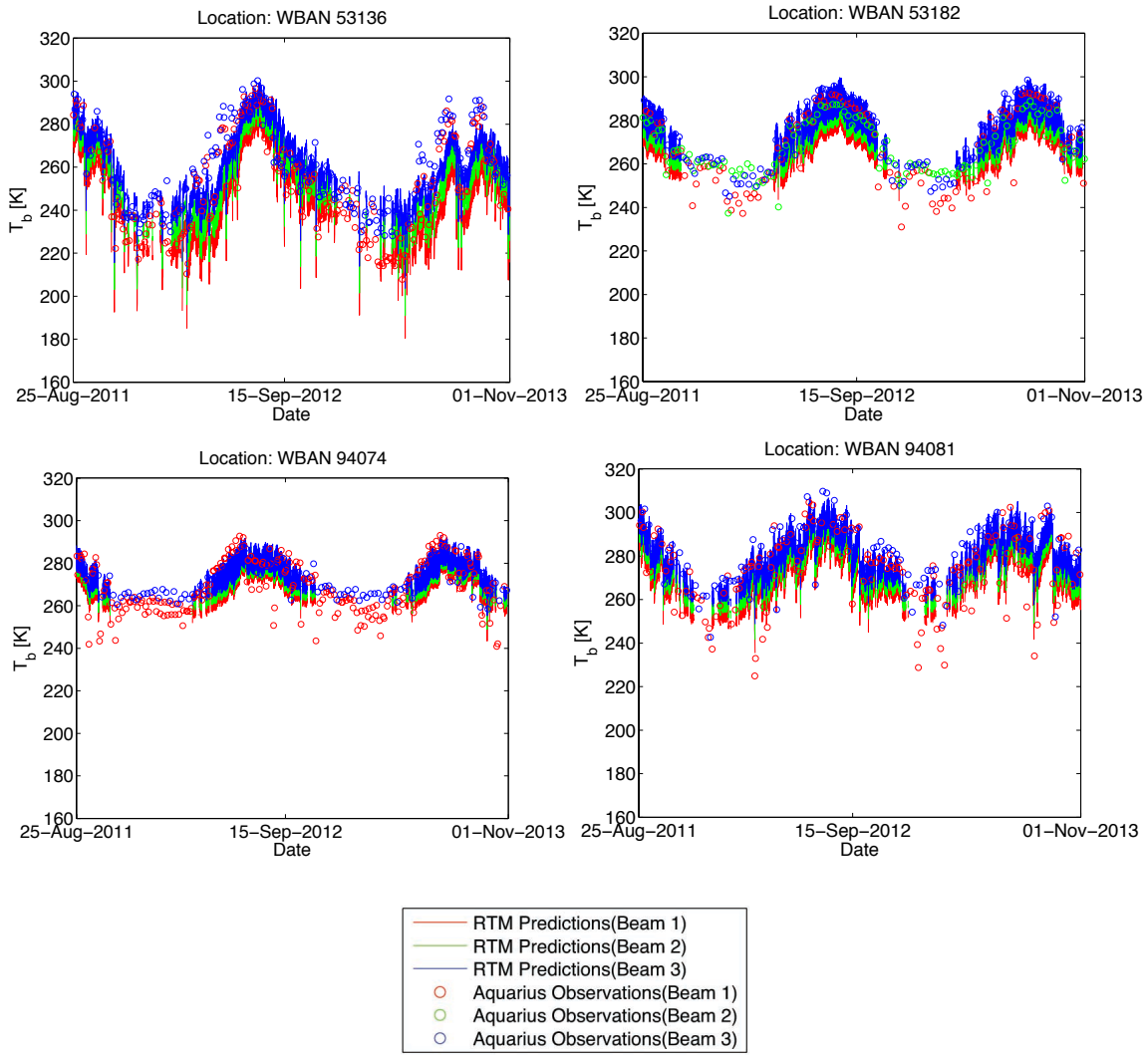

Figure 4-6: Time series plots for semi-arid climate (vertical polarization)

For semi-arid climate, Figure 4-5 and Figure 4-6 show time series for horizontal and vertical polarizations, respectively. Most of the study locations show higher variability in Tb both in the predictions and the observations in mountainous regions (study areas 53136, 4139, 4138, 22016). They show abrupt change in Tb resulting from sparse precipitation and rapid change in surface temperature variability between day and night. For both polarizations, Tb variability (standard deviation) is relatively higher in mountainous locations than for the other stations (Table 4-5 and Table 4-6). Most of the

region has low vegetation and bare soil with higher surface roughness that may affect the emission from the soil.

Table 4-5: Statistics for semi-arid climate (horizontal polarization)

WBAN	Beam	Mean Tb [K]		Standard Deviation [K]		Bias [K]	RMSE [K]	R [-]
		Aquarius	RTM	Aquarius	RTM			
53131	1	269.8	264.6	14.7	9.8	6.9	10.5	0.80
	2	N/A	N/A	N/A	N/A	N/A	N/A	N/A
	3	N/A	N/A	N/A	N/A	N/A	N/A	N/A
22016	1	236.5	234.2	24.8	21.1	7.9	15.1	0.85
	2	N/A	N/A	N/A	N/A	N/A	N/A	N/A
	3	226.1	228.2	24.6	23.7	4.1	13.5	0.85
3055	1	243.8	240.4	20.4	18.6	7.1	15.7	0.74
	2	242.3	237.1	17.9	19.4	10.9	17.2	0.77
	3	235.1	233.5	23.6	20.5	6.1	15.8	0.78
53182	1	N/A	N/A	N/A	N/A	N/A	N/A	N/A
	2	246.3	242.0	16.3	15.8	9.1	12.8	0.82
	3	N/A	N/A	N/A	N/A	N/A	N/A	N/A
94074	1	269.8	264.6	14.8	9.8	6.9	10.5	0.80
	2	N/A	N/A	N/A	N/A	N/A	N/A	N/A
	3	N/A	N/A	N/A	N/A	N/A	N/A	N/A
94081	1	252.2	250.5	6.6	5.1	4.4	5.1	0.91
	2	N/A	N/A	N/A	N/A	N/A	N/A	N/A
	3	248.6	245.5	6.6	6.5	6.5	6.9	0.93
4125	1	250.7	247.9	15.2	13.1	9.1	10.7	0.91
	2	N/A	N/A	N/A	N/A	N/A	N/A	N/A
	3	249.5	244.1	14.8	14.3	10.3	12.6	0.93
4138	1	236.4	234.7	24.7	21.3	7.6	15.5	0.83
	2	N/A	N/A	N/A	N/A	N/A	N/A	N/A
	3	226.2	227.5	24.7	22.7	5.6	13.8	0.86

N/A: Not Available (due to Aquarius measurements not falling within the spatial/temporal threshold)

Table 4-6: Statistics for semi-arid climate (vertical polarization)

WBAN	Beam	Mean Tb (K)		Standard Deviation (K)		Bias (K)	RMSE (K)	R (-)
		Aquarius	RTM	Aquarius	RTM			
53136	1	249.9	245.5	22.3	19.0	10.1	16.1	0.82
	2	N/A	N/A	N/A	N/A	N/A	N/A	N/A
	3	258.9	261.1	18.7	15.9	3.6	10.4	0.84
53131	1	277.4	273.2	13.3	9.3	5.7	8.7	0.83
	2	N/A	N/A	N/A	N/A	N/A	N/A	N/A
	3	N/A	N/A	N/A	N/A	N/A	N/A	N/A
22016	1	N/A	N/A	N/A	N/A	N/A	N/A	N/A
	2	267.8	267.3	12.0	7.8	10.6	11.7	0.88
	3	N/A	N/A	N/A	N/A	N/A	N/A	N/A
3055	1	259.2	262.3	9.2	8.0	7.3	9.7	0.68
	2	263.3	265.4	10.5	7.7	2.9	5.3	0.88
	3	263.5	268.9	7.8	7.2	4.7	6.0	0.87
53182	1	265.7	269.8	17.1	9.5	5.4	7.5	0.89
	2	265.7	273.7	18.5	9.2	8.0	9.1	0.84
	3	271.9	277.9	15.5	8.9	1.9	3.3	0.96
94074	1	268.3	271.2	12.1	7.5	5.3	9.7	0.57
	2	N/A	N/A	N/A	N/A	N/A	N/A	N/A
	3	271.2	276.4	7.4	6.6	4.5	6.9	0.54
94081	1	273.2	271.2	17.2	11.3	7.3	11.8	0.80
	2	N/A	N/A	N/A	N/A	N/A	N/A	N/A
	3	281.3	279.9	14.1	10.5	5.7	8.3	0.87
4125	1	278.7	276.7	14.6	10.0	5.0	12.8	0.60
	2	N/A	N/A	N/A	N/A	N/A	N/A	N/A
	3	287.7	283.1	10.2	9.8	7.2	7.7	0.95
4139	1	250.0	244.4	22.4	18.4	10.9	15.5	0.86
	2	N/A	N/A	N/A	N/A	N/A	N/A	N/A
	3	258.9	259.6	18.6	15.7	4.5	9.8	0.87

N/A: Not Available (due to Aquarius measurements not falling within the spatial/temporal threshold)

4.2.2 General Discussions on Evaluation of RTM

Results show that spatial heterogeneity (land surface condition) and local climate are key factors in soil moisture distribution and variability. Local climate is mostly dictated by the precipitation pattern and temperature variability, which affects the soil

moisture variability across space and time by controlling evaporative flux to the atmosphere from the near-surface soil moisture.

The performance of the RTM in Tb estimation appears to agree well with the Aquarius Tb observations. The mean estimates of Tb are within ~5K of the mean Aquarius observations. However, Aquarius observations contain more variability than the RTM estimates, which is evident from the higher standard deviation of the observations. The fluctuations are larger in semi-arid regions most likely due to sparse rainfall events in contrast to relatively consistent amounts of rainfall throughout the year in humid climate regions.

The Tb retrieval algorithm in the RTM produces some systematic errors and local biases. Higher Tb values (i.e., low soil moisture conditions) are underestimated by the RTM while lower Tb values (i.e., higher soil moisture conditions) better agree with the observations. Also, Tb estimation from semi-arid regions (limited amount of precipitation) produces a larger bias and RMSE compared to the other climate regions.

Other sources of systematic bias and RMSE may arise from the following:

(i) The RTM parameters are calibrated using SMOS observations. The parameters come from the GEOS-5 Catchment model on a 36-km EASE grid with forcing inputs from Modern-Era Retrospective Analysis for Research and Application (MERRA) at a spatial resolution of $\frac{1}{2}°$ x $\frac{2}{3}°$. On the other hand, Aquarius provides observations at spatial resolutions of 76 x 94 km (inner beam), 84 x 120 km (middle beam), and 96 x 156 km (outer beam). Moreover, Aquarius measurements are completely independent of SMOS measurements originally used during RTM

calibration. Therefore, uncertainty can be anticipated in the SMOS-calibrated RTM with respect to Aquarius observations.

(ii) The temporal threshold used to match Aquarius observations with the RTM was selected as 1.5 hours in order to calculate the statistics, which can result in the presence of representativeness (i.e., temporal mismatch) errors.

(iii) The Aquarius observations (and all observations in general) inherently contain random errors.

(iv) The backscattered microwave signal consists of signals from multiple sources in addition to soil moisture (e.g., overlying vegetation canopy, cloud cover, neighboring water bodies).

(v) The RTM does not provide Tb estimates during frozen soil conditions. When calculating bias and RMSE, the corresponding Aquarius measurements had to be excluded.

Land surface heterogeneity (e.g., roughness and vegetation) also impact passive microwave emission (Zribi et al., 2011) and cause variations in retrieved Tb. The time series plots for horizontal and vertical polarizations implicitly include land surface heterogeneity. In addition, seasonality plays an important role in characterizing soil moisture variability. The plots indicate higher soil moisture content during the late summer to winter and early spring (hence low Tb) and lower soil moisture content (high Tb) during the late spring and early summer. It is worth stating that part of the seasonality in the Tb observations (and RTM estimates) is associated with seasonal changes in the physical temperature of the land surface, which adds to the complexity of the mixed-

signal Tb values. That is, Tb variations show distinct seasonality, which is discussed in the next section.

4.3 Seasonal Analysis

The time series plots above (Figure 4-1 to Figure 4-6) clearly show seasonal variations of observed and estimated Tb from the Earth's surface. The emitted Tb is dependent on the surface emissivity and temperature. Climatic variations such as precipitation and temperature cause fluctuations in surface temperature associated with evaporative cooling of the surface soil moisture in conjunction with partitioning of the incident radiative flux. Seasonal analyses for different climate regions are discussed in the following subsections. Figure 4-7 to Figure 4-12 provide seasonal statistics (i.e., seasonal bias and RMSE) across the different climate regions.

4.3.1 Humid Continental/Cold Climate

Figure 4-7 and Figure 4-8 provide seasonal statistics for cold climate regions for horizontal and vertical polarizations, respectively. The majority of the plots in these figures show higher springtime seasonal bias and RMSE than for the other seasons of the year. Since winter is the wettest season of the year in these climate regions, precipitation and snowmelt contribute to the soil moisture storage, which is also highly dependent on the soil infiltration characteristics. Most of the region is also frozen during winter when RTM fails to estimate Tb, which can result in an inadequate sample size to compute relevant statistics. The RTM overestimates the Aquarius observations at all locations except at locations 4130 and 54811 during the summer. This underestimation is perhaps due to some low predictions of Tb immediately following precipitation events or due to strong attenuation from overlying vegetation.

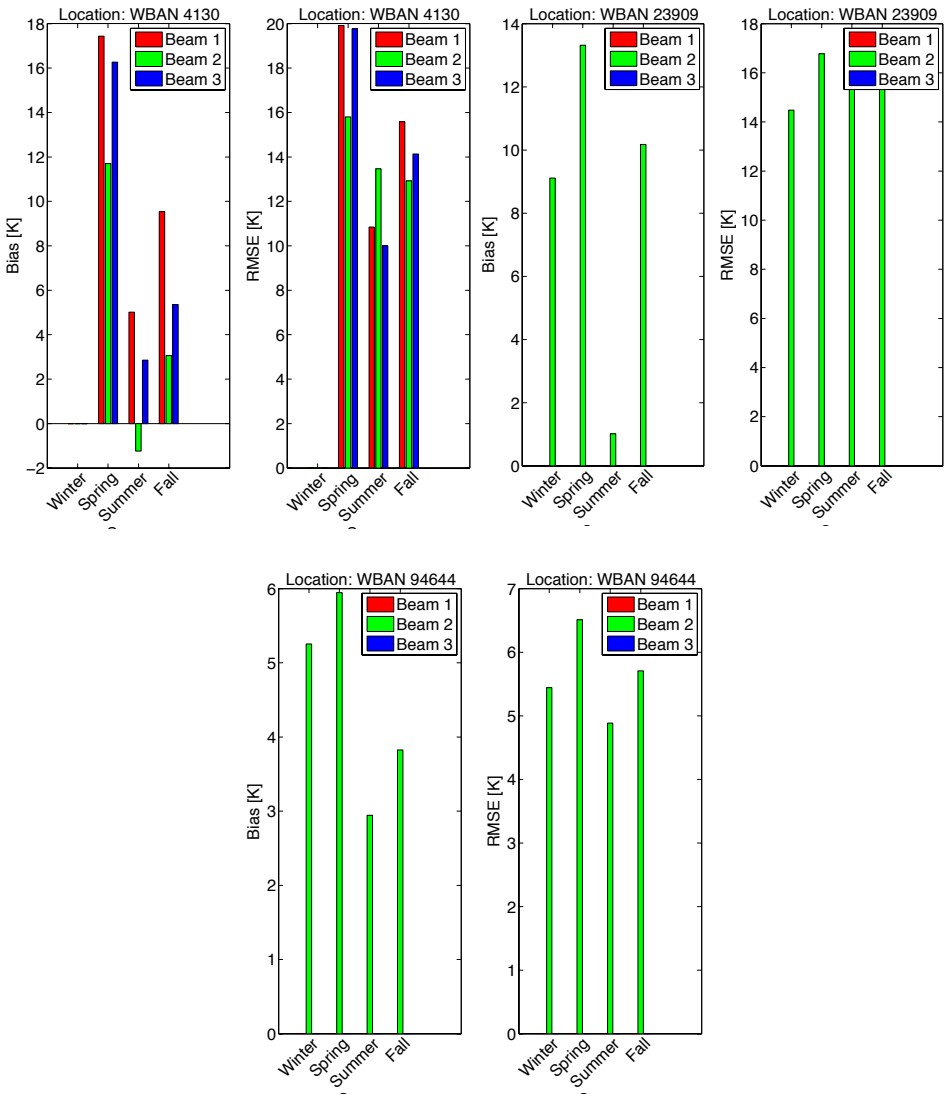

Figure 4-7: Seasonal statistics in humid continental/cold climate (horizontal polarization)

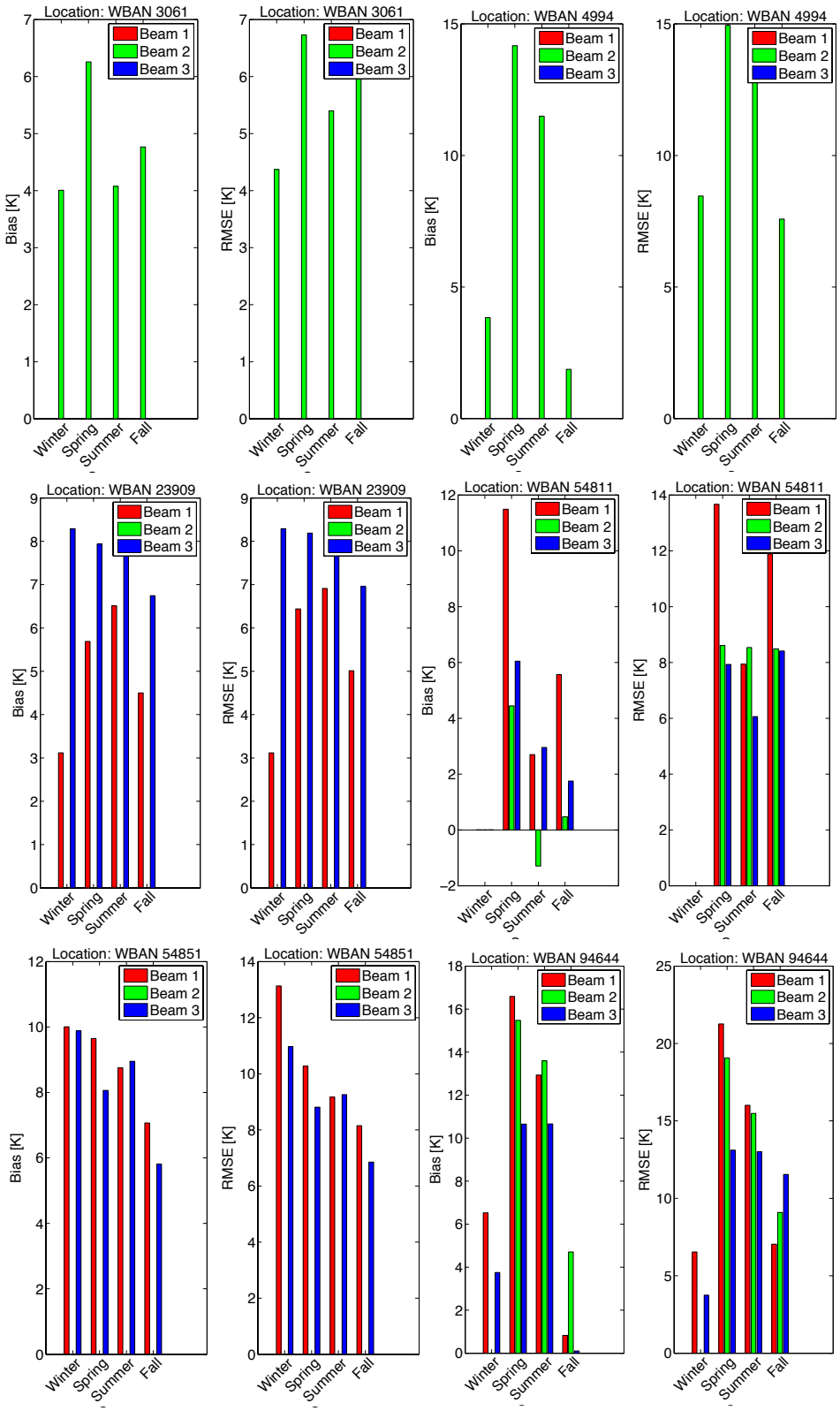

Figure 4-8: Seasonal statistics in humid continental/cold climate (vertical polarization)

4.3.2 Humid Subtropical Climate

Humid subtropical climate also shows a similar seasonal pattern as the humid continental or cold climate with springtime high positive bias and RMSE. Possible reasons may include influence erroneous precipitation forcing, inadequate soil parameterizations, or vegetation cover or optically-thin vegetation estimates employed by the RTM. The locations 23908, and 92826 (Figure 4-9 and Figure 4-10) underestimate beam 3 predictions in summer. In general, summertime biases and RMSEs are low compared to those in other seasons, which may be associated with better estimates of vegetation characteristics and/or precipitation forcing.

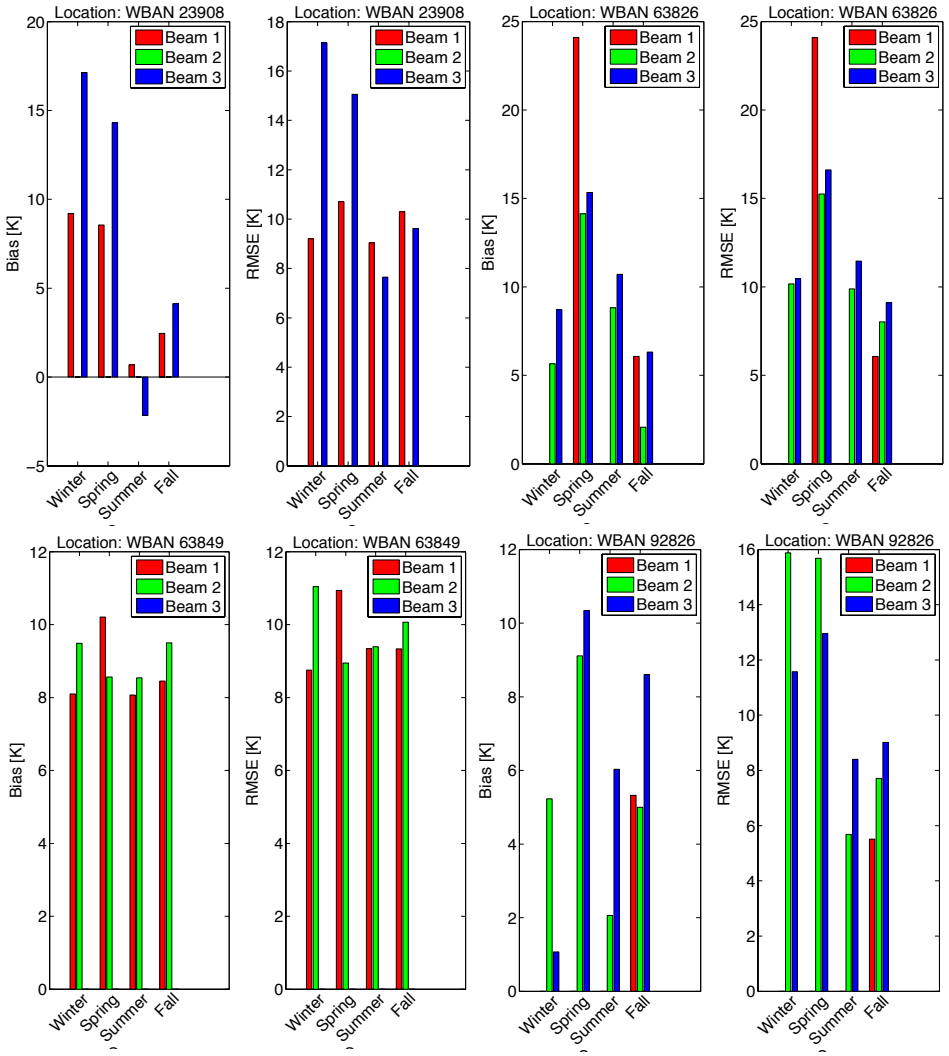

Figure 4-9: Seasonal statistics in humid subtropical climate (horizontal polarization)

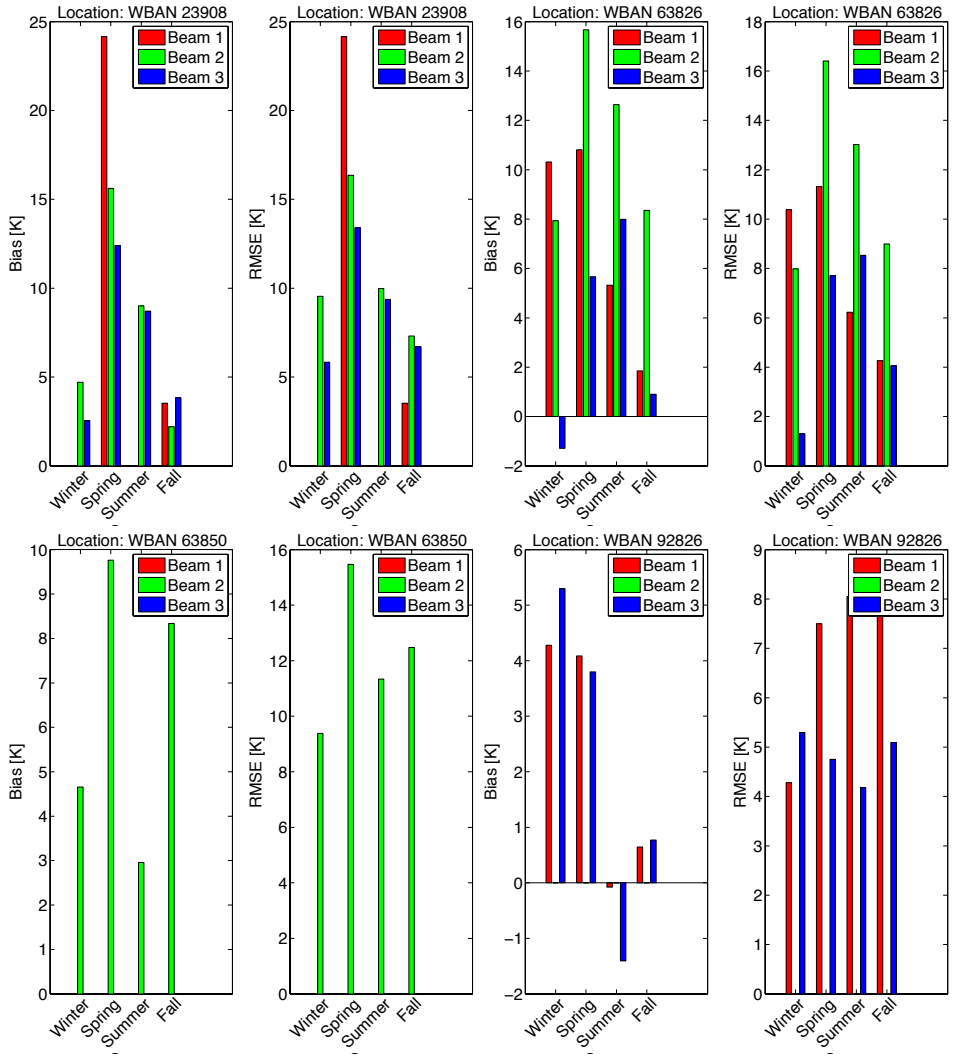

Figure 4-10: Seasonal statistics in humid subtropical climate (vertical polarization)

4.3.3 Semi-Arid Climate

In the continental United States, semi-arid climates are generally hot with a dry summer and very cold winter with relatively little snow in most regions. Often located at higher elevations, these climates generate large changes in diurnal temperature. Here, seasonal statistics also show higher extent of errors compared to other climate regions. In general, variance increases with the increase of mean soil moisture content in semi-arid regions (Lawrence and Hornberger, 2007). High forest density and topographical

complexity is a characteristic in these regions. Forest density and vegetation type play a significant role in attenuating the PMW signal from the Earth's surface. Therefore, larger error is expected in these region where RTM overestimates the observations. In addition, bare soil can contribute to an underestimation by the RTM in some locations (e.g., site 3055, Oklahoma Panhandle Research and Extension Center, OK; site 4138, Golden Spike National Historic Site Visitor Center, UT; site 53136, Desert Rock Meteorological Laboratory, NV). For vertical polarization (Figure 4-12), its sensitivity to surface temperature may result in relatively lower bias than horizontally polarized observations.

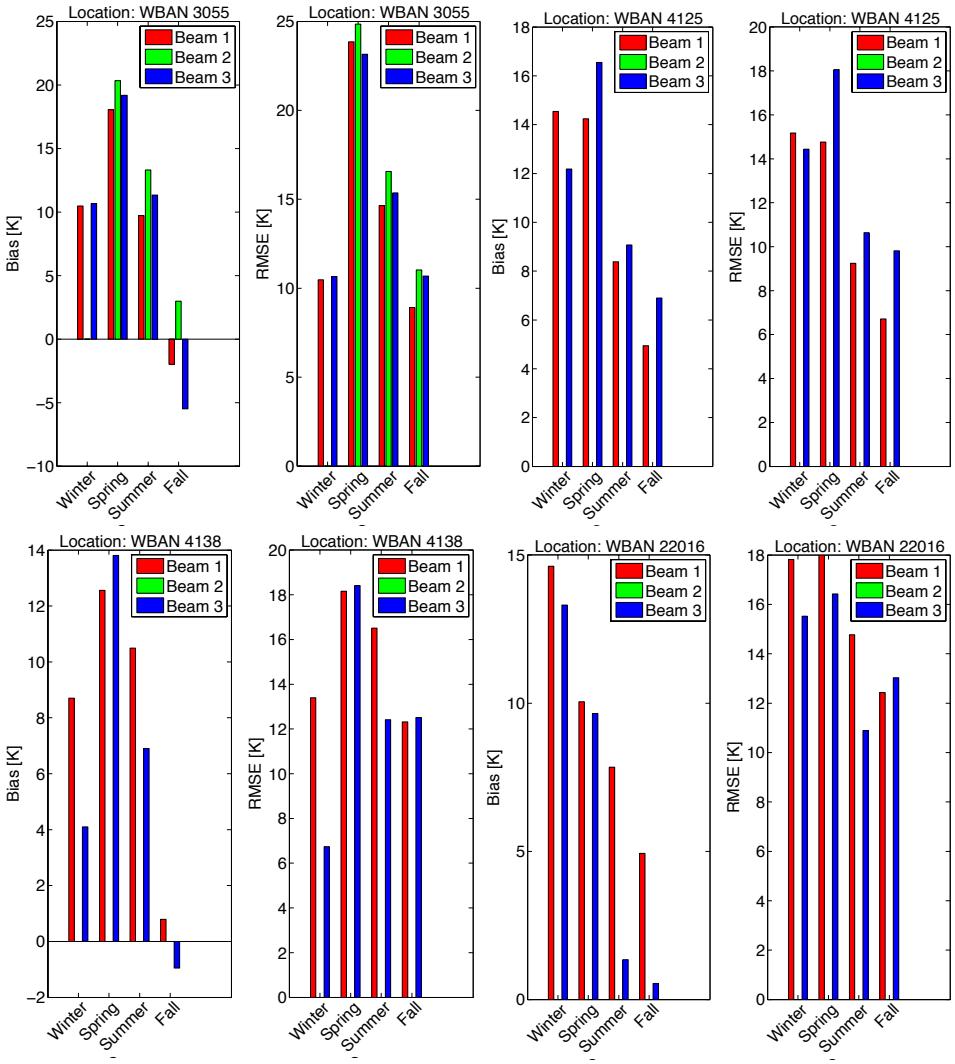

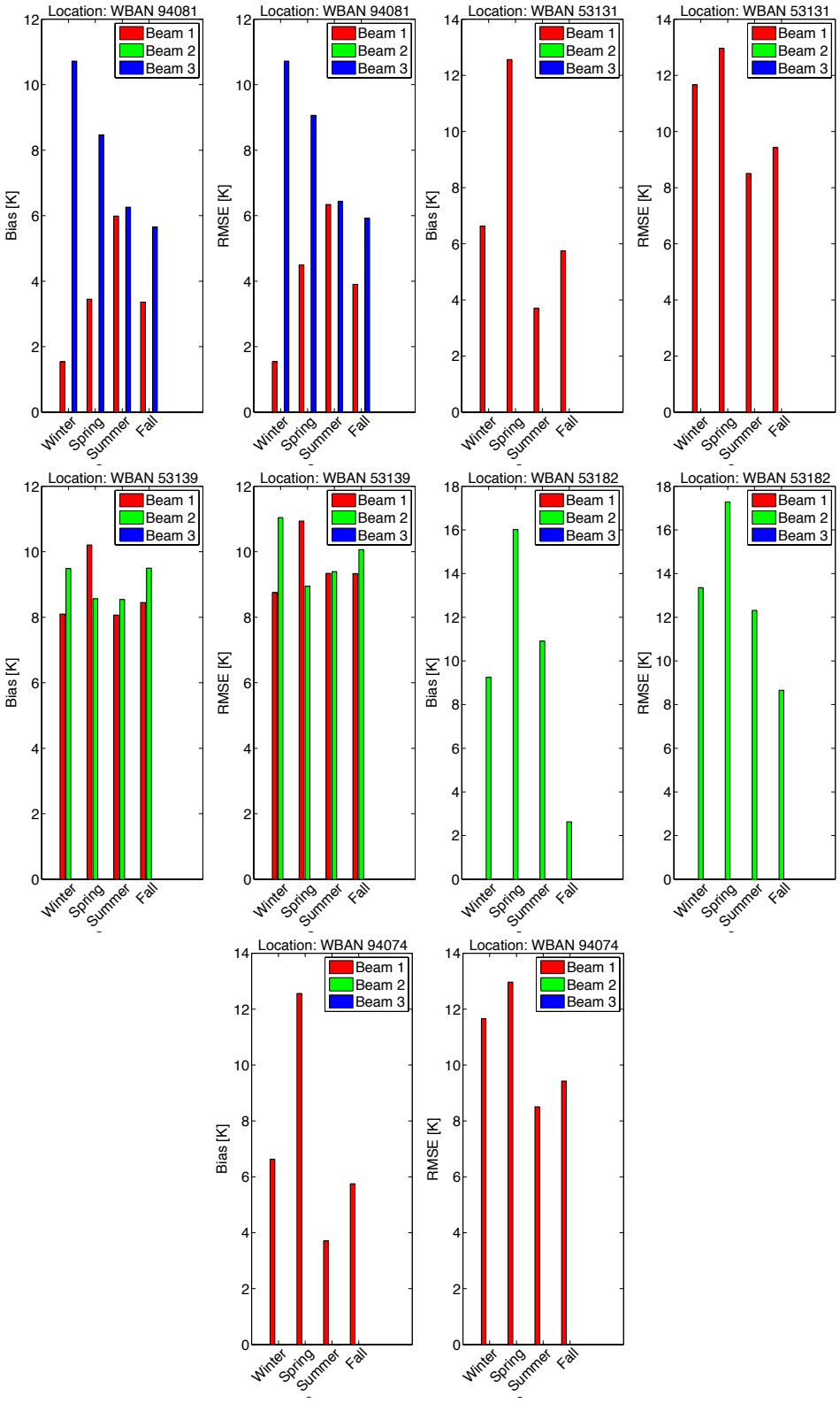

Figure 4-11: Seasonal statistics for semi-arid climate (horizontal polarization)

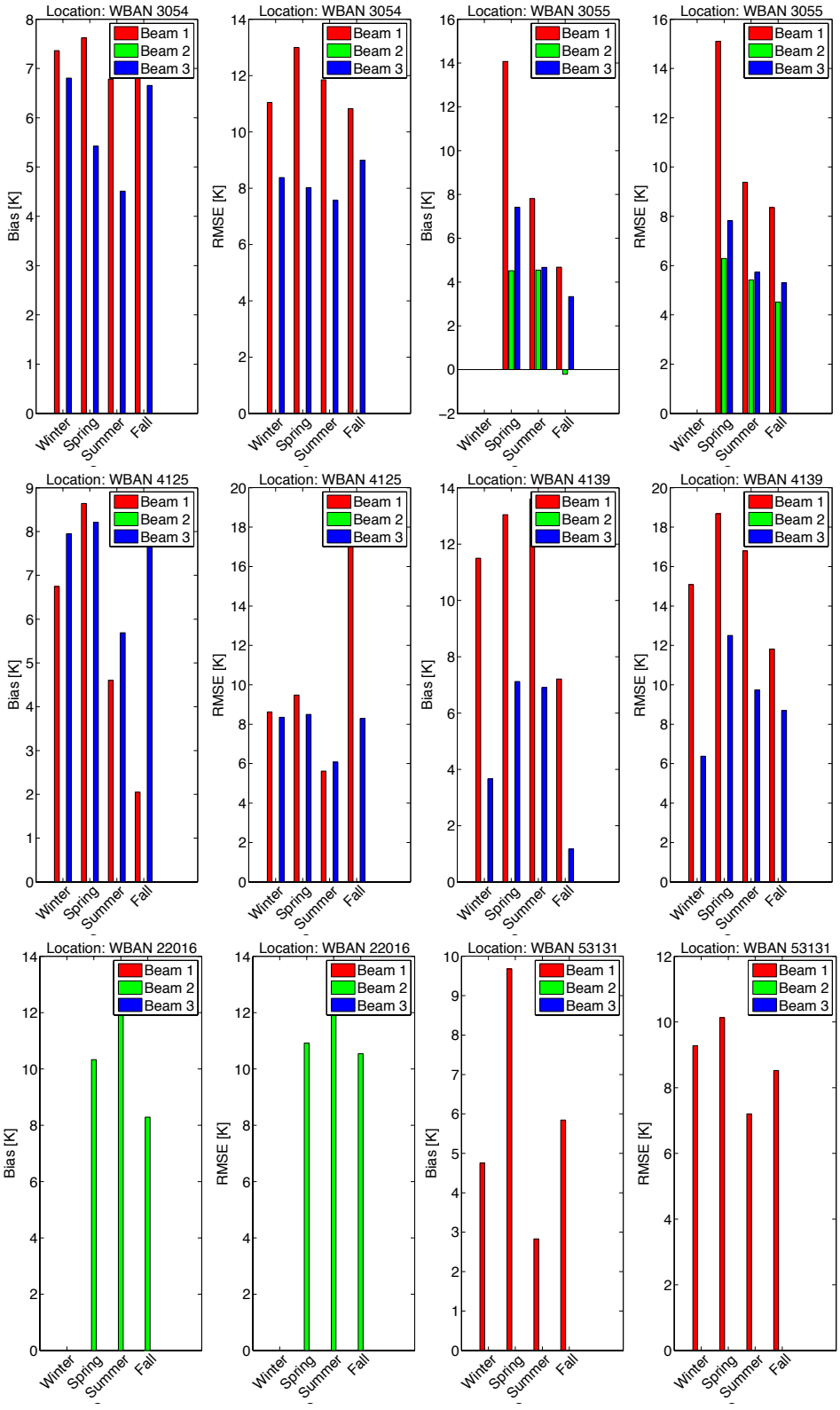
Location: WBAN 3054
Bias [K]
Location: WBAN 3054
RMSE [K]
Location: WBAN 3055
Bias [K]
Location: WBAN 3055
RMSE [K]
Location: WBAN 4125
Bias [K]
Location: WBAN 4125
RMSE [K]
Location: WBAN 4139
Bias [K]
Location: WBAN 4139
RMSE [K]
Location: WBAN 22016
Bias [K]
Location: WBAN 22016
RMSE [K]
Location: WBAN 53131
Bias [K]
Location: WBAN 53131
RMSE [K]
Beam 1
Beam 2
Beam 3
Winter
Spring
Summer
Fall

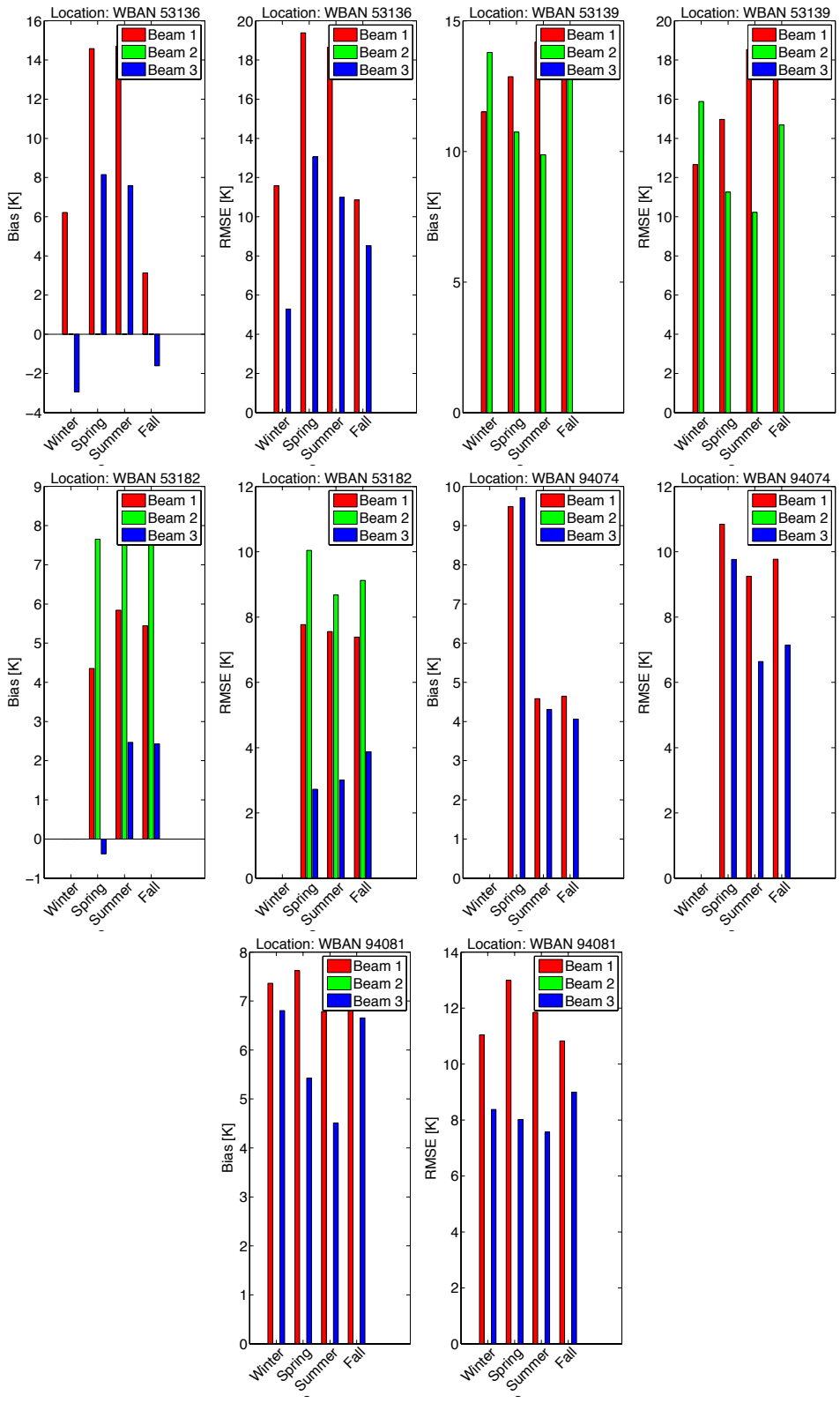

Figure 4-12: Seasonal statistics in semi-arid climate (vertical polarization)

For semi-arid climate, most of the study area has high springtime bias in Tb. In some places, the summer and fall seasons have as large of a bias as during the spring. Temperature and precipitation play a key role in determining soil water storage and evaporation. Unlike the precipitation pattern in humid continental or humid subtropical climates, the amount of total precipitation is much less here, which may cause a reduction in soil water content resulting in similar type of systematic bias all the year round.

Again, the passive microwave signature from the Earth surface is not entirely based on soil moisture content. Other factors such as vegetation water content, water bodies, and soil type can alter the emission of in the microwave spectrum that is inferred as Tb by the radiometer on board a satellite. The fact that the RTM is calibrated against SMOS is also another probable cause of error and uncertainty in the Tb estimates.

4.4 Aquarius Time Series Comparison with USCRN

USCRN stations provide volumetric water content (VWC) at multiple depths. Time series comparison with the USCRN measurements is a useful means of checking the consistency of Tb measurements. Moreover, precipitation data are provided with USCRN data to further evaluate the Tb response.

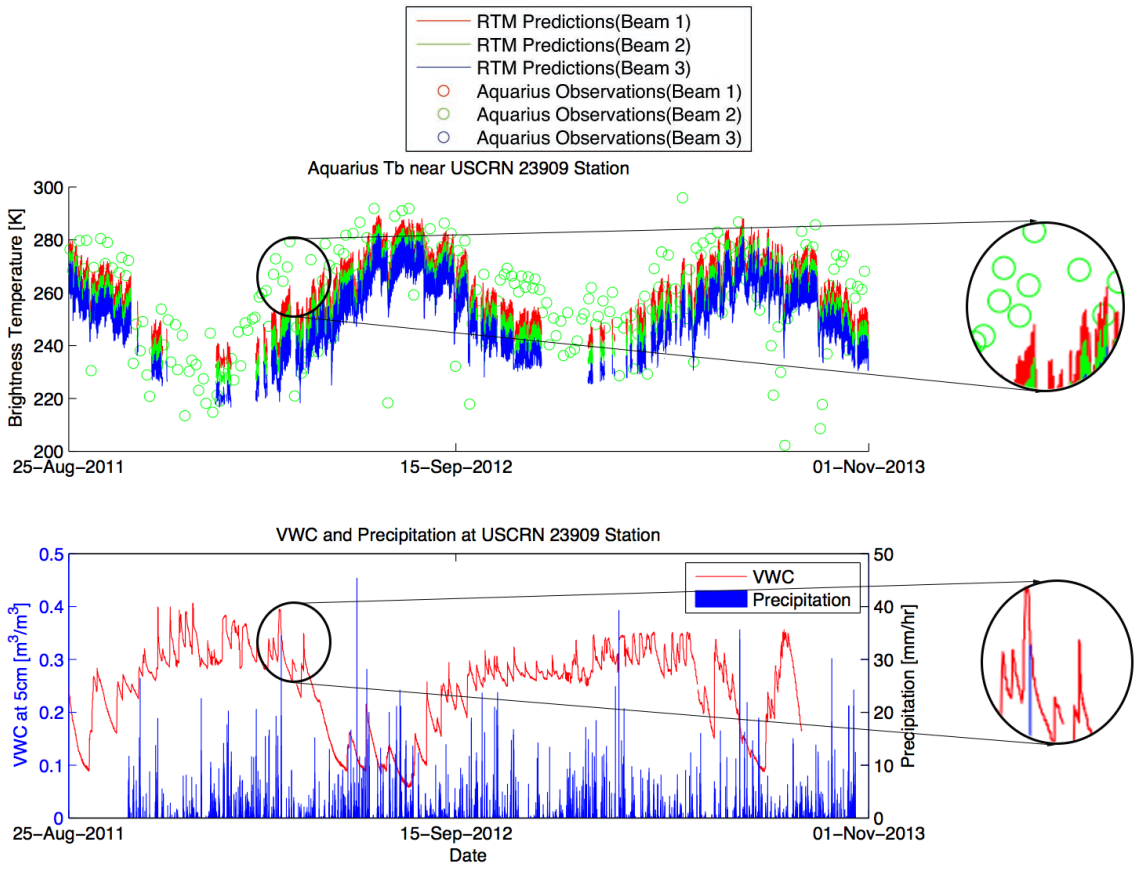

Figure 4-13: USCRN VWC and Aquarius Tb time series comparison at USCRN 23909 station in humid continental climate

Figure 4-13 shows near-surface VWC variability with precipitation inputs as recorded at the USCRN 23909 station along corresponding Tb signal within the distance threshold of 0.5-degrees. Near-surface soil moisture shows high variability and responds immediately with the external precipitation forcing. External atmospheric fluxes that are responsible for its dynamics are precipitation and evaporation from soil. Nearby Tb observations from Aquarius in the time series shows the response of the Earth's surface emission with the soil moisture variability. Lower Tb observations are associated with higher VWC (in the range approximately between 0.25 to 0.4 m^3/m^3) and higher Tb observations correspond to lower VWC (in the range approximately between 0.08 to 0.2

m^3/m^3). The effect of precipitation also affects the nearby Tb signal as it results in a reduction in the Aquarius observations. The zoomed in portions in the Figure 4-13 shows a closer view of the Tb response with the variations in soil moisture and the effect of precipitation.

The RTM variability also captures the soil moisture variability except for the frozen land conditions and some precipitation events. Since the model utilizes inputs from the Catchment model, which is forced with MERRA forcing, it does not always perform well at capturing individual precipitation events. The lack of accurate precipitation inputs at all times could, in part, result in erroneous RTM estimates.

Chapter 5: Conclusions and Future Recommendations

5.1 Summary and Limitation of the Study

Although soil moisture accounts for only a small part of the global hydrologic cycle (Oki and Kanae, 2006), its importance in land-atmosphere interactions cannot be neglected, since it is the main driver of the evaporative flux from the land surface.

This study evaluates the zero-order tau-omega NASA RTM with respect to Aquarius Tb observations. The RTM parameters are preprocessed so that they provide L-band Tb predictions over non-frozen soil condition. The performance of the NASA RTM is assessed based on Aquarius Tb observations across portions of the continental United States. The RTM is calibrated against ESA SMOS observations, therefore some discrepancy exists between the Aquarius observations and the SMOS-calibrated RTM predictions. The key points from the results show that:

i. Soil moisture variability is largely controlled by spatial heterogeneity (land surface conditions such as surface roughness, vegetation type, soil type) and local climatology (precipitation pattern, temperature variability) throughout the year.
ii. The RTM performs reasonably well when compared to the Aquarius observations with mean estimates of Tb within ~5K of the mean Aquarius Tb values. Some systematic biases in the RTM predictions do exist.
iii. The time series plots show that the RTM underestimates high Tb values (i.e., low soil moisture conditions) while lower Tb values (i.e., higher soil moisture conditions) agree better with Aquarius Tb.

iv. Seasonal variations were observed in the Aquarius Tb observations and the RTM Tb predictions.

v. Other factors that may contribute to the seasonal variations in Tb are vegetation cover and vegetation type. Vegetation cover is highly dynamic in time. L-band frequency is semi-transparent to moderate vegetation and does not perform well in dense forest cover.

vi. Springtime Tb overestimates the observations in humid continental and humid subtropical climates. This is partially due to relatively small sample sizes available from the RTM for comparison with Aquarius Tb observations due to frozen soil conditions.

vii. In semi-arid climate, relatively larger variations (i.e., larger uncertainty) in Aquarius Tb observations and RTM Tb predictions were found due to higher temperature anomalies and irregular precipitation patterns. Surface heterogeneity (i.e., variations in elevations, vegetation pattern) plays a crucial role in these regions.

Soil moisture anomaly does not cause variations in Tb predictions or observations alone. More factors such as soil roughness, soil types (compaction and infiltration properties), and vegetation cover type also contributes to the PMW signal. This study does not cover these issues, which is a limitation to the Tb estimate from the RTM. Another limitation of the study is the fact that the influence of soil type on soil moisture content was not investigated. The influence of soil type and compaction determine the soil infiltration characteristics which is a major contributor to the soil water content (Miller et al., 2002) and hence PMW emission. Another important limitation of the study

is the frozen soil state during which the RTM is not capable of predicting PMW Tb. This limitation resulted in the removal (masking) of Aquarius Tbs during the quality control check in order to ensure consistency with the RTM output.

5.2 Recommendation for Future Study

Since PMW signature from the Earth's surface is a function of numerous factors, it is of great interest to study the contribution from individual components. For example, more work is needed to investigate the relationship between PMW Tb and soil type. Similarly, more work is needed to investigate the role of vegetation type and vegetation cover dynamics on PMW Tb estimation.

The overarching goal of this study is to integrate model and observations into the data assimilation framework to better estimate soil moisture. Data assimilation has been used extensively in hydrologic science in order to enhance our knowledge of the hydrologic system. Since measurements and models contain error (and uncertainty), work needs to be conducted in order to reduce this error (and uncertainty)

References

Ahmad, S., Kalra, A., Stephen, H., 2010. Estimating soil moisture using remote sensing data: A machine learning approach. Adv. Water Resour. 33, 69–80. doi:10.1016/j.advwatres.2009.10.008

Al Bitar, A., Leroux, D., Kerr, Y.H., Merlin, O., Richaume, P., Sahoo, A., Wood, E.F., 2012. Evaluation of SMOS Soil Moisture Products Over Continental U.S. Using the SCAN/SNOTEL Network. IEEE Trans. Geosci. Remote Sens. 50, 1572–1586. doi:10.1109/TGRS.2012.2186581

Ayyub, B.M., McCuen, R.H., 2011. Probability, Statistics, and Reliability for Engineers and Scientists, Third Edition. Taylor & Francis, Boca Raton, FL 33487-2742.

Bell, J.E., Palecki, M.A., Baker, C.B., Collins, W.G., Lawrimore, J.H., Leeper, R.D., Hall, M.E., Kochendorfer, J., Meyers, T.P., Wilson, T., Diamond, H.J., 2013. U.S. Climate Reference Network Soil Moisture and Temperature Observations. J. Hydrometeorol. 14, 977–988.

Brocca, L., Moramarco, T., Melone, F., Wagner, W., 2013a. A new method for rainfall estimation through soil moisture observations. Geophys. Res. Lett. 40, 853–858. doi:10.1002/grl.50173

Brocca, L., Zucco, G., Moramarco, T., Morbidelli, R., 2013b. Developing and testing a long-term soil moisture dataset at the catchment scale. J. Hydrol. 490, 144–151. doi:10.1016/j.jhydrol.2013.03.029

Brubaker, K.L., Entekhabi, D., 1995. An Analytic Approach to Modeling Land-Atmosphere Interaction: 1. Construct and Equilibrium Behavior. Water Resour. Res. 31, 619–632. doi:10.1029/94WR01772

Calvet, J.-C., Noilhan, J., Bessemoulin, P., 1998. Retrieving the Root-Zone Soil Moisture from Surface Soil Moisture or Temperature Estimates: A Feasibility Study Based on Field Measurements. J. Appl. Meteorol. 37, 371–386. doi:10.1175/1520-0450(1998)037<0371:RTRZSM>2.0.CO;2

Cashion, J., Lakshmi, V., Bosch, D., Jackson, T.J., 2005. Microwave remote sensing of soil moisture: evaluation of the TRMM microwave imager (TMI) satellite for the Little River Watershed Tifton, Georgia. J. Hydrol. 307, 242–253. doi:10.1016/j.jhydrol.2004.10.019

Chaouch, N., Leconte, R., Magagi, R., Temimi, M., Khanbilvardi, R., 2013. Multi-Stage Inversion Method to Retrieve Soil Moisture from Passive Microwave Measurements over the Mackenzie River Basin. Vadose Zo. J. 1–38. doi:10.2136/vzj2012.0134

Choudhury, B.J., Schmugge, T.J., Chang, A., Newton, R.W., 1979. Effect of surface roughness on the microwave emission from soils. J. Geophys. Res. 84, 5699. doi:10.1029/JC084iC09p05699

Corradini, C., 2014. Soil moisture in the development of hydrological processes and its determination at different spatial scales. J. Hydrol. doi:10.1016/j.jhydrol.2014.02.051

Crow, W.T., Wood, E.F., 2005. The assimilation of remotely sensed soil brightness temperature imagery into a land surface model using Ensemble Kalman filtering : a case study based on ESTAR measurements during SGP97. Adv. Water Resour. 26, 137–149.

De Lannoy, G.J.M., Reichle, R.H., Pauwels, V.R.N., 2013. Global Calibration of the GEOS-5 L-Band Microwave Radiative Transfer Model over Nonfrozen Land Using SMOS Observations. J. Hydrometeorol. 14, 765–785. doi:10.1175/JHM-D-12-092.1

Delworth, T., Manabe, S., 1989. The influence of soil wetness on near-surface atmospheric variability. J. Clim. 2, 1447–1462.

Dirmeyer, P.A., Jin, Y., Singh, B., Yan, X., 2013. Trends in Land–Atmosphere Interactions from CMIP5 Simulations. J. Hydrometeorol. 14, 829–849. doi:10.1175/JHM-D-12-0107.1

Dorigo, W.A., Scipal, K., Parinussa, R.M., Liu, Y.Y., Wagner, W., de Jeu, R.A.M., Naeimi, V., 2010. Error characterisation of global active and passive microwave soil moisture datasets. Hydrol. Earth Syst. Sci. 14, 2605–2616. doi:10.5194/hess-14-2605-2010

Entekhabi, D., Njoku, E.G., O'Neill, P.E., Kellogg, K.H., Crow, W.T., Edelstein, W.N., Entin, J.K., Goodman, S.D., Jackson, T.J., Johnson, J., Kimball, J., Piepmeier, J.R., Koster, R.D., Martin, N., McDonald, K.C., Moghaddam, M., Moran, S., Reichle, R., Shi, J.C., Spencer, M.W., Thurman, S.W., Tsang, L., Van Zyl, J., 2010. The Soil

Moisture Active Passive (SMAP) Mission. Proc. IEEE 98, 704–716. doi:10.1109/JPROC.2010.2043918

Entekhabi, D., Rodriguez-Iturbe, I., Castelli, F., 1996. Mutual interaction of soil moisture state and atmospheric processes. J. Hydrol. 184, 3–17.

Famiglietti, J.S., Devereaux, C.A., Laymont, C.A., Tsegaye, T., Houser, P.R., Jackson, T.J., Graham, S.T., Rodell, M., van Oevelen, P.J., 1999. Ground-based investigation of soil moisture variability within remote sensing footprints during the Southern Great Plains 1997 (SGP97) Hydrology Experiment. Water Resour. Res. 35, 1839–1851.

Fang, B., Lakshmi, V., 2013. Soil moisture at watershed scale: Remote sensing techniques. J. Hydrol. doi:10.1016/j.jhydrol.2013.12.008

Forman, B.A., Reichle, R.H., Rodell, M., 2012. Assimilation of terrestrial water storage from GRACE in a snow-dominated basin. Water Resour. Res. 48, W01507. doi:10.1029/2011WR011239

Guo, Z., Dirmeyer, P.A., DelSole, T., Koster, R.D., 2012. Rebound in Atmospheric Predictability and the Role of the Land Surface. J. Clim. 25, 4744–4749. doi:10.1175/JCLI-D-11-00651.1

Guo, Z., Dirmeyer, P.A., Koster, R.D., Sud, Y.C., Bonan, G., Oleson, K.W., Chan, E., Verseghy, D., Cox, P., Gordon, C.T., McGregor, J.L., Kanae, S., Kowalczyk, E., Lawrence, D., Liu, P., Mocko, D., Lu, C.-H., Mitchell, K., Malyshev, S.,

McAvaney, B., Oki, T., Yamada, T., Pitman, A., Taylor, C.M., Vasic, R., Xue, Y., 2006. GLACE: The Global Land–Atmosphere Coupling Experiment. Part II: Analysis. J. Hydrometeorol. 7, 611–625. doi:10.1175/JHM511.1

Heim, R.R., 2001. New network to monitor climate change. Eos, Trans. Am. Geophys. Union 82, 143. doi:10.1029/EO082i012p00143

Hillel, D., 1998. Environmental Soil Physics. Academic Press, San Diego.

Hong, S.-Y., Pan, H.-L., 2000. Impact of soil moisture anomalies on seasonal, summertime circulation over North America in a Regional Climate Model. J. Geophys. Res. 105, 29625. doi:10.1029/2000JD900276

Houser, P.R., Shuttleworth, W.J., Famiglietti, J.S., Gupta, H. V., Syed, K.H., Goodrich, D.C., 1998. Integration of soil moisture remote sensing and hydrologic modeling using data assimilation. Water Resour. Res. 34, 3405–3420. doi:10.1029/1998WR900001

Jackson, T.J., 1993. Measuring surface soil moisture using passive microwave remote sensing. Hydrol. Process. 7, 139–152. doi:10.1002/hyp.3360070205

Jackson, T.J., 2001. Multiple Resolution Analysis of L-Band Brightness Temperature for Soil Moisture. IEEE Trans. Geosci. Remote Sens. 39, 151–164.

Jackson, T.J., Bindlish, R., Cosh, M.H., Zhao, T., Starks, P.J., Bosch, D.D., Seyfried, M., Moran, M.S., Goodrich, D.C., Kerr, Y.H., Leroux, D., 2012. Validation of Soil Moisture and Ocean Salinity (SMOS) Soil Moisture Over Watershed Networks in

the U.S. IEEE Trans. Geosci. Remote Sens. 50, 1530–1543. doi:10.1109/TGRS.2011.2168533

Jackson, T.J., Schmugge, T.J., 1989. Passive Microwave Remote Sensing System for Soil Moisture: Some Supporting Research. IEEE Trans. Geosci. Remote Sens. 27.

Jackson, T.J., Schmugge, T.J., 1991. Vegetation effects on the microwave emission of soils. Remote Sens. Environ. 36, 203–212. doi:10.1016/0034-4257(91)90057-D

Jackson, T.J., Schmugge, T.J., Wang, J.R., 1982. Passive microwave sensing of soil moisture under vegetation canopies. Water Resour. Res. 18, 1137–1142. doi:10.1029/WR018i004p01137

Jensen, J.R., 2007. Remote Sensing Of The Environment: An Earth Resource Perspective, Prentice Hall Series in Geographic Information Science. Pearson Prentice Hall.

Jury, W.A., Gardner, W.R., Gardner, W.H., 1991. Soil Physics. John Wiley and Sons Inc., New York.

Kerr, Y.H., Waldteufel, P., Wigneron, J.-P., Martinuzzi, J., Font, J., Berger, M., 2001. Soil moisture retrieval from space: the Soil Moisture and Ocean Salinity (SMOS) mission. IEEE Trans. Geosci. Remote Sens. 39, 1729–1735. doi:10.1109/36.942551

Kerr, Y.H., Wigneron, J., Delwart, S., Cabot, F., Boutin, J., Escorihuela, M.-J., Font, J., Reul, N., Gruhier, C., Juglea, S.E., Drinkwater, M.R., Hahne, A., Martin-Neira, M.,

Mecklenburg, S., 2010. The SMOS Mission: New Tool for Monitoring Key Elements of the Global Water Cycle. Proc. IEEE 98, 666–687.

Koblinsky, C.J., Hildebrand, P., LeVine, D., Pellerano, F., Chao, Y., Wilson, W., Yueh, S., Lagerloef, G., 2003. Sea surface salinity from space: Science goals and measurement approach. Radio Sci. 38. doi:10.1029/2001RS002584

Koppen, W., 1936. Das geographische System der Klimate. Handb. der Klimatologie 1–44.

Koster, R.D., Dirmeyer, P.A., Guo, Z., Bonan, G., Chan, E., Cox, P., Gordon, C.T., Kanae, S., Kowalczyk, E., Lawrence, D., Liu, P., Lu, C.-H., Malyshev, S., McAvaney, B., Mitchell, K., Mocko, D., Oki, T., Oleson, K., Pitman, A., Sud, Y.C., Taylor, C.M., Verseghy, D., Vasic, R., Xue, Y., Yamada, T., 2004. Regions of strong coupling between soil moisture and precipitation. Science (80-.). 305, 1138–40. doi:10.1126/science.1100217

Koster, R.D., Mahanama, S.P.P., Livneh, B., Lettenmaier, D.P., Reichle, R.H., 2010. Skill in streamflow forecasts derived from large-scale estimates of soil moisture and snow. Nat. Geosci. 3, 613–616. doi:10.1038/ngeo944

Koster, R.D., Mahanama, S.P.P., Yamada, T.J., Balsamo, G., Berg, A.A., Boisserie, M., Dirmeyer, P.A., Doblas-Reyes, F.J., Drewitt, G., Gordon, C.T., Guo, Z., Jeong, J.-H., Lee, W.-S., Li, Z., Luo, L., Malyshev, S., Merryfield, W.J., Seneviratne, S.I., Stanelle, T., van den Hurk, B.J.J.M., Vitart, F., Wood, E.F., 2011. The Second Phase of the Global Land–Atmosphere Coupling Experiment: Soil Moisture Contributions

to Subseasonal Forecast Skill. J. Hydrometeorol. 12, 805–822. doi:10.1175/2011JHM1365.1

Koster, R.D., Suarez, M.J., Ducharne, A., Stieglitz, M., Kumar, P., 2000. A catchment-based approach to modeling land surface processes in a general circulation model structure. J. Geophys. Res. 105, 24809–24822.

Koster, R.D., Suarez, M.J., Higgins, R.W., Van den Dool, H.M., 2003. Observational evidence that soil moisture variations affect precipitation. Geophys. Res. Lett. 30. doi:10.1029/2002GL016571

Koster, R.D., Sud, Y.C., Guo, Z., Dirmeyer, P.A., Bonan, G., Oleson, K.W., Chan, E., Verseghy, D., Cox, P., Davies, H., Kowalczyk, E., Gordon, C.T., Kanae, S., Lawrence, D., Liu, P., Mocko, D., Lu, C.-H., Mitchell, K., Malyshev, S., McAvaney, B., Oki, T., Yamada, T., Pitman, A., Taylor, C.M., Vasic, R., Xue, Y., 2006. GLACE: The Global Land–Atmosphere Coupling Experiment. Part I: Overview. J. Hydrometeorol. 7, 590–610. doi:10.1175/JHM510.1

Kottek, M., Grieser, J., Beck, C., Rudolf, B., Rubel, F., 2006. World Map of the Köppen-Geiger climate classification updated. Meteorol. Zeitschrift 15, 259–263. doi:10.1127/0941-2948/2006/0130

Kutilek, M., Nielsen, D.R., 1994. Soil Hydrology. Catena-Verlag, Cremlingen-Destedt.

Lawrence, J.E., Hornberger, G.M., 2007. Soil moisture variability across climate zones. Geophys. Res. Lett. 34, L20402. doi:10.1029/2007GL031382

Le Vine, D.M., Lagerloef, G.S.E., Colomb, F.R., Yueh, S.H., Member, S., Pellerano, F.A., 2007. Aquarius : An Instrument to Monitor Sea Surface Salinity From Space. IEEE Trans. Geosci. Remote Sens. 45, 2040–2050.

Leroux, D.J., Kerr, Y.H., Bitar, A. Al, Bindlish, R., Member, S., Jackson, T.J., Berthelot, B., Portet, G., 2013. Comparison Between SMOS , VUA , ASCAT , and ECMWF Soil Moisture Prodcuts Over Four Watersheds in U.S. IEEE Trans. Geosci. Remote Sens. 1–10.

Leroux, D.J., Kerr, Y.H., Wood, E.F., Sahoo, A.K., Bindlish, R., Jackson, T.J., 2014. An Approach to Constructing a Homogeneous Time Series of Soil Moisture Using SMOS. IEEE Trans. Geosci. Remote Sens. 52, 393–405. doi:10.1109/TGRS.2013.2240691

Li, L., Njoku, E.G., Im, E., Chang, P.S., St.Germain, K., 2004. A Preliminary Survey of Radio-Frequency Interference Over the U.S. in Aqua AMSR-E Data. IEEE Trans. Geosci. Remote Sens. 42, 380–390. doi:10.1109/TGRS.2003.817195

Lukas, R., Lindstrom, E., 1991. The mixed layer of the western equatorial Pacific Ocean. J. Geophys. Res. 96, 3343. doi:10.1029/90JC01951

Margulis, S. a., McLaughlin, D., Entekhabi, D., Dunne, S., 2002. Land data assimilation and estimation of soil moisture using measurements from the Southern Great Plains 1997 Field Experiment. Water Resour. Res. 38, 35–1–35–18. doi:10.1029/2001WR001114

McKnight, T.L., Hess, D., 2000. Climate zones and types: the Köppen system, in: Physical Geography: A Landscape Appreciation. Prentice Hall, Upper Saddle River, NJ.

McLaughlin, D., 2002. An integrated approach to hydrologic data assimilation: interpolation, smoothing, and filtering. Adv. Water Resour. 25, 1275–1286. doi:10.1016/S0309-1708(02)00055-6

Miller, C.J., Yesiller, N., Yaldo, K., Merayyan, S., 2002. Impact of Soil Type and Compaction Conditions on Soil Water Characteristic. Am. Soc. Civ. Eng.

Montzka, C., Grant, J.P., Moradkhani, H., Franssen, H.-J.H., Weihermüller, L., Drusch, M., Vereecken, H., 2013. Estimation of radiative transfer parameters from L-band passive microwave brightness temperatures using advanced data assimilation. Vadose Zo. J. 12.

Moradkhani, H., 2008. Hydrologic remote sensing and land surface data assimilation. Sensors 8, 2986–3004.

Njoku, E.G., Ashcroft, P., Chan, T.K., 2005. Global survey and statistics of radio-frequency interference in AMSR-E land observations. IEEE Trans. Geosci. Remote Sens. 43, 938–947. doi:10.1109/TGRS.2004.837507

Njoku, E.G., Entekhabi, D., 1996. Passive microwave remote sensing of soil moisture. J. Hydrol. 184, 101–129. doi:http://dx.doi.org/10.1016/0022-1694(95)02970-2

Oki, T., Kanae, S., 2006. Global hydrological cycles and world water resources. Science (80-.). 313, 1068–72. doi:10.1126/science.1128845

Owe, M., de Jeu, R., Walker, J., 2001. A methodology for surface soil moisture and vegetation optical depth retrieval using the microwave polarization difference index. IEEE Trans. Geosci. Remote Sens. 39, 1643–1654. doi:10.1109/36.942542

Palecki, M.A., Bell, J.E., 2013. U.S. Climate Reference Network Soil Moisture Observations with Triple Redundancy: Measurement Variability. Vadose Zo. J. 12. doi:10.2136/vzj2012.0158

Pampaloni, P., Paloscia, S., 1986. Microwave Emission and Plant Water Content: A Comparison between Field Measurements and Theory. IEEE Trans. Geosci. Remote Sens. GE-24, 900–905. doi:10.1109/TGRS.1986.289705

Pan, F., Peters-Lidard, C.D., Sale, M.J., 2003. An analytical method for predicting surface soil moisture from rainfall observations. Water Resour. Res. 39, n/a–n/a. doi:10.1029/2003WR002142

Peel, M., 2007. Updated world map of the Köppen-Geiger climate classification. Hydrol. Earth Syst. Sci. 11, 1633–1644.

Pellarin, T., Wigneron, J.-P., Calvet, J.-C., Berger, M., Douville, H., Ferrazzoli, P., Kerr, Y.H., Lopez-Baeza, E., Pulliainen, J., Simmonds, L.P., Waldteufel, P., 2003. Two-year global simulation of L-band brightness temperatures over land. IEEE Trans. Geosci. Remote Sens. 41, 2135–2139. doi:10.1109/TGRS.2003.815417

Qiu, J., Mo, X., Liu, S., Lin, Z., Yang, L., Song, X., Zhang, G., Naeimi, V., Wagner, W., 2013. Intercomparison of microwave remote-sensing soil moisture data sets based on distributed eco-hydrological model simulation and in situ measurements over the North China Plain. Int. J. Remote Sens. 1–24. doi:10.1080/01431161.2013.788799

Reichle, R.H., McLaughlin, D.B., Entekhabi, D., 2002. Hydrologic Data Assimilation with the Ensemble Kalman Filter. Mon. Weather Rev. 130, 103–114. doi:10.1175/1520-0493(2002)130<0103:HDAWTE>2.0.CO;2

Robinson, D.A., Campbell, C.S., Hopmans, J.W., Hornbuckle, B.K., Jones, S.B., Knight, R., Ogden, F., Selker, J., Wendroth, O., 2008. Soil Moisture Measurements for Ecological and Hydrological Watershed Scale Observatories: A Review. Vadose Zo. J. 7, 358–389.

Robock, A., Vinnikov, K.Y., Srinivasa, G., Entin, J.K., Hollinger, S.E., Speranskaya, N.A., Liu, S., Namkhai, A., Srinivasan, G., 2000. The Global Soil Moisture Data Bank. Bull. Am. Meteorol. Soc. 81, 1281–1299. doi:10.1175/1520-0477(2000)081<1281:TGSMDB>2.3.CO;2

Sahoo, A.K., De Lannoy, G.J.M., Reichle, R.H., Houser, P.R., 2013. Assimilation and downscaling of satellite observed soil moisture over the Little River Experimental Watershed in Georgia, USA. Adv. Water Resour. 52, 19–33. doi:10.1016/j.advwatres.2012.08.007

Santanello, J. a., Peters-Lidard, C.D., Kennedy, A., Kumar, S. V., 2013. Diagnosing the Nature of Land–Atmosphere Coupling: A Case Study of Dry/Wet Extremes in the

U.S. Southern Great Plains. J. Hydrometeorol. 14, 3–24. doi:10.1175/JHM-D-12-023.1

Schaefer, G.L., Cosh, M.H., Jackson, T.J., 2007. The USDA Natural Resources Conservation Service Soil Climate Analysis Network (SCAN). J. Atmos. Ocean. Technol. 24, 2073–2077. doi:10.1175/2007JTECHA930.1

Schmugge, T.J., Jackson, T.J., 1993. Passive microwave remote sensing of soil moisture. EARSeL Adv. Remote Sens. 2.

Schmugge, T.J., Kustas, W.P., Ritchie, J.C., Jackson, T.J., Rango, A., 2002. Remote sensing in hydrology. Adv. Water Resour. 25, 1367–1385. doi:10.1016/S0309-1708(02)00065-9

Schultz, G.A., Engman, E.T., 2000. Remote sensing in hydrology and water management. Springer Berlin etc.

Seneviratne, S.I., Corti, T., Davin, E.L., Hirschi, M., Jaeger, E.B., Lehner, I., Orlowsky, B., Teuling, A.J., 2010. Investigating soil moisture–climate interactions in a changing climate: A review. Earth-Science Rev. 99, 125–161. doi:10.1016/j.earscirev.2010.02.004

Seneviratne, S.I., Lüthi, D., Litschi, M., Schär, C., 2006. Land-atmosphere coupling and climate change in Europe. Nature 443, 205–9. doi:10.1038/nature05095

Shuttleworth, W.J., 2012. Terrestrial Hydrometeorology. Wiley.

Su, C.-H., Ryu, D., Young, R.I., Western, A.W., Wagner, W., 2013. Inter-comparison of microwave satellite soil moisture retrievals over the Murrumbidgee Basin, southeast Australia. Remote Sens. Environ. 134, 1–11. doi:10.1016/j.rse.2013.02.016

Thornthwaite, C.W., 1948. An Approach toward a Rational Classification of Climate. Geogr. Rev. 38, 55–94 CR – Copyright © 1948 American Geograph. doi:10.2307/210739

Tindall, J.A., Kunkel, J.R., 1999. Unsaturated Zone Hydrology for Scientists and Engineers. Prentice Hall, Upper Saddle River.

Tsang, L., Newton, R.W., 1982. Microwave emissions from soils with rough surfaces. J. Geophys. Res. 87, 9017. doi:10.1029/JC087iC11p09017

Tsang, L., Njoku, E., Kong, J.A., 1975. Microwave thermal emission from a stratified medium with nonuniform temperature distribution. J. Appl. Phys. 46, 5127. doi:10.1063/1.321571

Vose, R.S., Easterling, D.R., Karl, T.R., Helfert, M., 2005. Comments on “Microclimate Exposures of Surface-Based Weather Stations”. Bull. Am. Meteorol. Soc. 86, 504–506. doi:10.1175/BAMS-86-4-504

Vose, R.S., Menne, M.J., 2004. A Method to Determine Station Density Requirements for Climate Observing Networks. J. Clim. 17, 2961–2971. doi:10.1175/1520-0442(2004)017<2961:AMTDSD>2.0.CO;2

Walker, J.P., Houser, P.R., 2001. A methodology for initializing soil moisture in a global climate model: Assimilation of near-surface soil moisture observations. J. Geophys. Res. Atmos. 106, 11761–11774. doi:10.1029/2001JD900149

Wang, J.R., Choudhury, B.J., 1981. Remote sensing of soil moisture content, over bare field at 1.4 GHz frequency. J. Geophys. Res. 86, 5277. doi:10.1029/JC086iC06p05277

Xia, Y., Sheffield, J., Ek, M., Dong, J., Chaney, N., Wei, H., Meng, J., Wood, E.F., 2014. Evaluation of Multi-Model Simulated Soil Moisture in NLDAS-2. J. Hydrol.

Zaitchik, B.F., Santanello, J.A., Kumar, S. V., Peters-Lidard, C.D., 2013. Representation of Soil Moisture Feedbacks during Drought in NASA Unified WRF (NU-WRF). J. Hydrometeorol. 14, 360–367. doi:10.1175/JHM-D-12-069.1

Zribi, M., Chahbi, A., Shabou, M., Lili-Chabaane, Z., Duchemin, B., Baghdadi, N., Amri, R., Chehbouni, A., 2011. Soil surface moisture estimation over a semi-arid region using ENVISAT ASAR radar data for soil evaporation evaluation. Hydrol. Earth Syst. Sci. 15, 345–358. doi:10.5194/hess-15-345-2011